INVESTIGATION INTO ROUGHNESS CHARACTERISTICS BY MEASURING ANGULAR DISTRIBUTION USING He-Ne LASER

A Thesis Submitted

in partial fulfilment of the requirements

of the Degree of

MASTER OF TECHNOLOGY

by

RAJNISH KASHYAP

to the

LASER TECHNOLOGY PROGRAMME

INDIAN INSTITUTE OF TECHNOLOGY KANPUR

MAY, 1990

CERTIFICATE

It is certified that the work contained in the thesis entitled **Investigation into Roughness Characteristics by Measuring Angular Distribution using He-Ne Laser** by Mr Rajnish Kashyap, has been carried out under our supervision and that this work has not been submitted elsewhere for a degree.

(K K Sharma)
Professor and Head
Laser Technology Programme
Indian Institute of Technology,
Kanpur 208 016

(G S Kainth)
Professor
Deptt of Mechanical Engineering
Indian Institute of Technology,
Kanpur 208 016

May, 1990

LTP-1990-M- KAS-ℐNV

ACKNOWLEDGEMENT

And finally as a token of respect , I thank my father .M.M.Kashyap , my mother Mrs.U.Kashyap for their constant encouragement,inspiration,love and affection bestowed during the whole course of my stay here.

                                        Kashyap.R

TABLE OF CONTENTS

LIST OF FIGURES

LIST OF TABLES

NOMENCLATURE

AD	Angular Distribution
α	Change in Angle of Incidence (Ch.3)
I_s	Specular Intensity
k	Propagation Vector = $2\Pi/\lambda$
λ	Wavelength of He-Ne Laser = 6328.193 A^o
Λ	Spatial Wavelength of Roughness
R	Reflection Coefficient
R_a	Roughness Average
Ratio	Λ/λ
ρ	Amplitude Scattering Coefficient
R_{15}	Ratio of Specular Intensity to Intensity in 15° Off-Specular Direction
rss	Rough Surface Specimen
R_N	Nose Radius of the Tool
θ_i, θ_1	Angle of Incidence w.r.t Normal
θ_s	Scattering Angle w.r.t θ_i
θ_2	Scattering Angle w.r.t Normal

Name   : Kashyap , R.

Roll No.   : 8811606

Programme   : M.Tech./Laser Technology

Thesis Title   : Investigation Into Roughness Characteristics by

                  Measuring Angular Distribution Using He-Ne Laser.

Thesis Supervisor   : Dr.G.S.Kainth and Dr.K.K.Sharma

ABSTRACT

Almost all the modern machining processes involve removal of material from a surface to give it desired shape and size. The resulting removal process creates a profile on the surface which is the cause of roughness of the surface .

A rough surface scatters a collimated beam of laser light according to the laws of physical optics. The intensity and pattern of scattered light depends upon roughness height, spatial wavelength of roughness , wavelength of incident light and angle of incidence. Lasers , because of their monochromaticity , directionality and high power density , offer a potential tool for the measurement of surface roughness. Measurement of surface roughness using lasers come under the heading of parametric technique, which involves measuring a parameter that represents some property of surface topography averaged over the illuminated area.

In the present work effort has been done to measure surface roughness of highly periodic aluminium surface by using He-Ne laser. The scattered light is assumed to be a diffraction

pattern obtained by a periodic diffraction grating of constant amplitude and wavelength . The resulting diffraction pattern consists of fine diffraction spots. The separation of diffraction spots depends upon spatial wavelength of roughness and intensity depends upon the roughness heights.

Angular distrbution (AD) of scattered light is measured for various angle of incidence for face turned and face milled aluminium specimens by an instrument designed and fabricated in CELT workshop.

Angular distribution for all specimens show a No. of peaks. However, the experimental spacing is much higher than the theoretical spacing. Therefore, it is not possible to relate peak spacing to spatial wavelength of roughness.

Variation of specular intensity I_s show that all surfaces tend to reflect most of the incident light specularly at near grazing angle of incidence. The variation of I_s with roughness shows that I_s decreases with roughness. The decrease is much steeper for $\theta_i = 85^\circ$ than for $\theta_i = 87.5^\circ$. Approximate logarithmic expression has been calculated which shows that I_s can be used for measuring R_a ranging from 0.3μ to 1.0μ at near grazing angle of incidence of 85°.

CHAPTER 1

INTRODUCTION AND LITERATURE SURVEY

1.1 INTRODUCTION

Almost all the modern machining processes involve removal of material from a surface to give it desired shape and size. The resulting material removal process creates a profile on the surface, the shape of profile being characterized by particular cutting process and cutting conditions. The generated profile may be considered as a form of 3-dimensional geometric irregularity from the intended perfectly smooth surface. The order of irregularity determines the amount of roughness of a surface. The following four orders of geometrical irregularities are recognised in standards (Fig.1.1) [1].

I-order : Arising out of inaccuracies in machine tool, deformation of a work under the cutting forces or the weight of material itself.

II-order : Caused by vibrations of machine or workpiece.

III-order: Caused by machining itself and characteristic of the process.

IV-order : Arising from rupture of material during chip removal.

1.2 DEFINITIONS OF TERMS

The following are the definitions of terms used for the study of roughness of a surface. The *surface* of an object is the boundry which separates that object from another object, substance or space. The *nominal surface* is the .intended surface contour
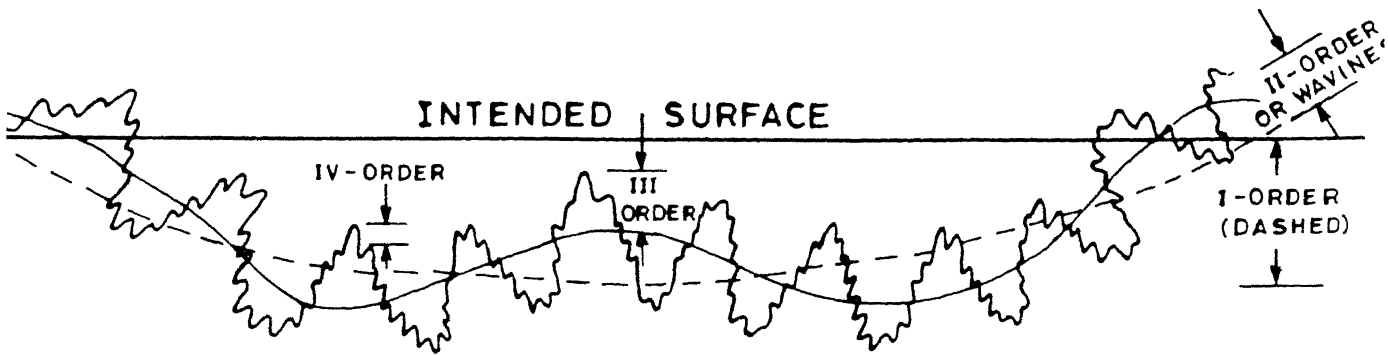
FIG. 1.1 FOUR ORDERS OF GEOMETRIC IRREGULARITIES.
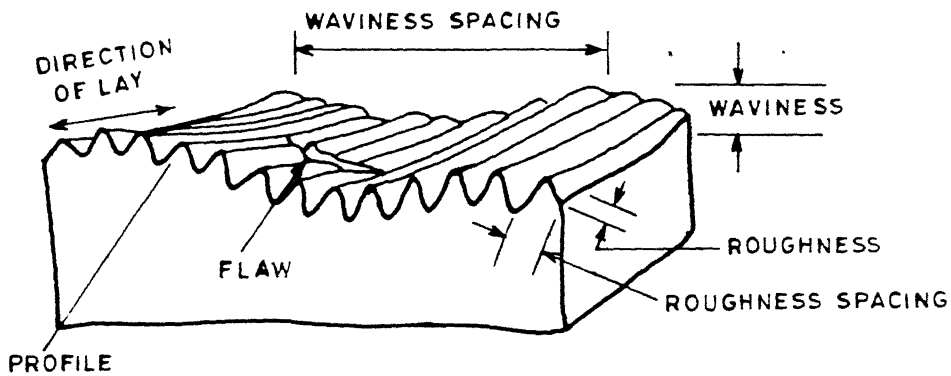
FIG. 1.2 SURFACE CHARACTERISTICS.
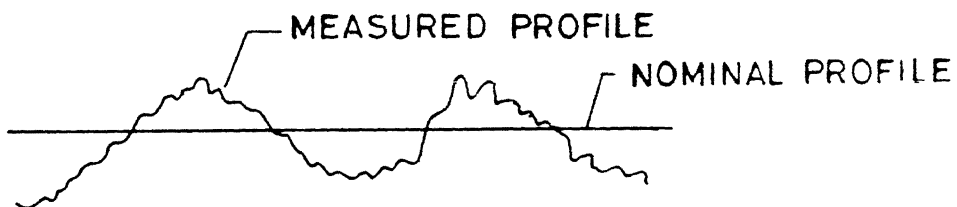
FIG. 1.3 NOMINAL AND MEASURED PROFILE.

(excluding any surface roughness), the shape and extent of which is usually shown and dimensioned on a drawing or descriptive specification. *Surface texture* is the repetitive or random deviations from the nominal surface which forms the three dimensional topography of the surface. Surface texture includes roughness, waviness, lay and flaws (Fig.1.2). *Roughness* consists of finer irregularities of surface texture which are inherent in production processes. *Waviness* is the more widely spaced component of surface texture upon which roughness is superimposed. *Lay* is the direction of predominant surface pattern, ordinarily determined by the production method. *Flaws* are unintentional, unexpected and unwanted interruptions in the topography. The *profile* is the contour of the surface in a plane perpendicular to the surface, unless some other angle is specified. The *nominal profile* is a profile of the nominal surface. It is the intended profile exclusive of any roughness. The *measured profile* is a representation of the profile obtained by instrumental or other means (Fig.1.3). The *graphical centreline* or the *meanline* (Fig.1.4-b) is the line about which roughness is measured and is a line parallel to the general direction of profile within the limits of sampling length L, such that the sum of areas embraced by the surface profile above the line are equal to sum of those below it. That is,

$$\sum (A_1 + A_3 + A_5 + \ldots) = \sum (A_2 + A_4 + A_6 + \ldots)$$

A *peak* is the point of maximum height on that portion of a profile that lies above the centreline and between two interactions of the profile with the centreline and a *valley* is the point of maximum depth on the portion of the profile which lies below the

centreline and between two interactions of profile with centreline
(Fig.1.4-b).

1.3 PARAMETERS

Engineering surfaces are produced by a wide variety of
processes resulting in variation of profile. A milled surface,
for example, has a strong lay pattern, whereas, a bead blasted
surface is isotropic (i.e. roughness measured along any direction
is constant) and its structure is highly random. Most engineering
surfaces, however, have a certain degree of anisotropy and
combination of both periodic and random features. To quantify
surface roughness a number of statistical functions and parameters
have been developed. These characterize two basic aspects of
topography, the height of asperties (amplitude) and longitudinal
spacing between the asperities (spatial wavelength). For
simplicity the definitions are expressed in terms of two
dimensional surface profile Z(x). However there are equivalent
three dimensional expressions also. Assuming that profile at a
crossection AA' (Fig. 1.4-a) be some curve defined by $Z = f(x)$,
then:

ROUGHNESS AVERAGE R_a (also known as centreline average (CLA) or
arithmatic average (AA)) represents the average deviation of
surface profile about its centreline, defined as

$$R_a = \frac{h_1 + h_2 + h_3 + \ldots\ldots + h_n}{L} = \frac{1}{L} \int_o^L |f(x)| dx$$

where   x = distance along the surface

           f(x) = height of surface profile about the centreline

           L = sampling length = beam dia. of laser at sample

RMS ROUGHNESS R_q (also known as σ in optics and statistics) is defined by

$$R_q = (\frac{1}{L} \int_0^L [f(x)]^2 dx)^{1/2}$$

where R_q = standard deviation of profile about the meanline. R_q is always greater than or equal to R_a.

.

AMPLITUDE DENSITY FUNCTION (ADF) is the probability density distribution of surface heights. It is found by plotting the histogram (Fig.1.5) of the profile points in vertical direction. If the surface is produced by truly random process, the ADF would be a Gaussian distribution of surface heights, given by:

$$ADF(Z) = (2\Pi R_q^2)^{1/2} \, e^{(-x^2/2R_q^2)}$$

POWER SPECTRAL DENSITY (PSD) caracterises both asperity amplitude and spacing, is calculated by fourier decomposition of surface.

$$PSD (f_x) = \frac{1}{L} | \int_0^L f(x) \, e^{-2\Pi f_x x} dx |^2$$

AUTOCORRELATION FUNCTION (ACF) is a quantitative measure of the similarity between the laterally shifted and unshifted version of the profile. It also characterizes both wavelength and amplitude properties of a surface.

$$ACF(\tau) = \frac{1}{L} \int_0^L f(x) \, f(x+\tau) dx$$
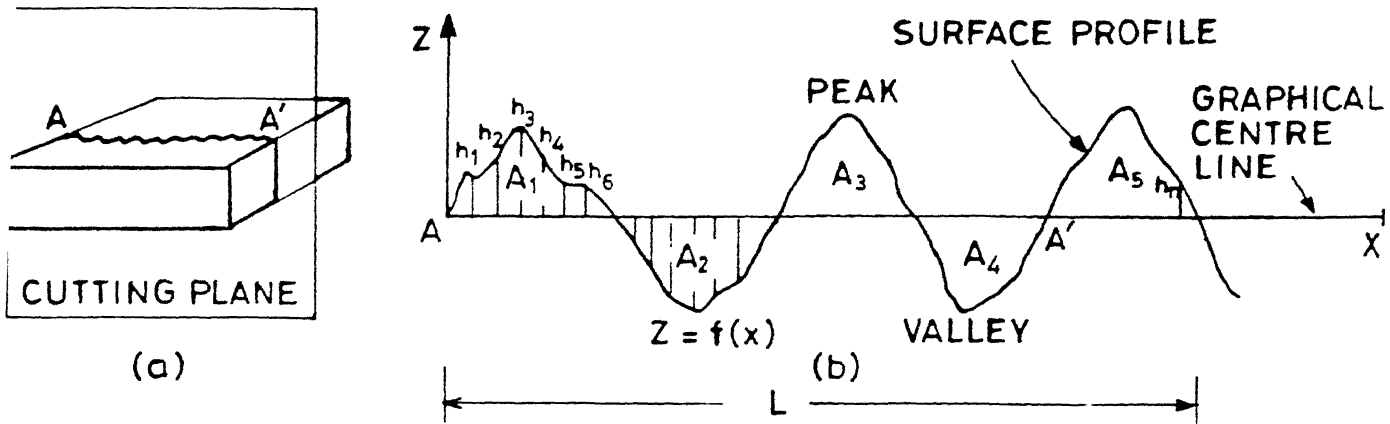
FIG. 1.4 DEFINITION OF CENTRELINE OR MEAN LINE.
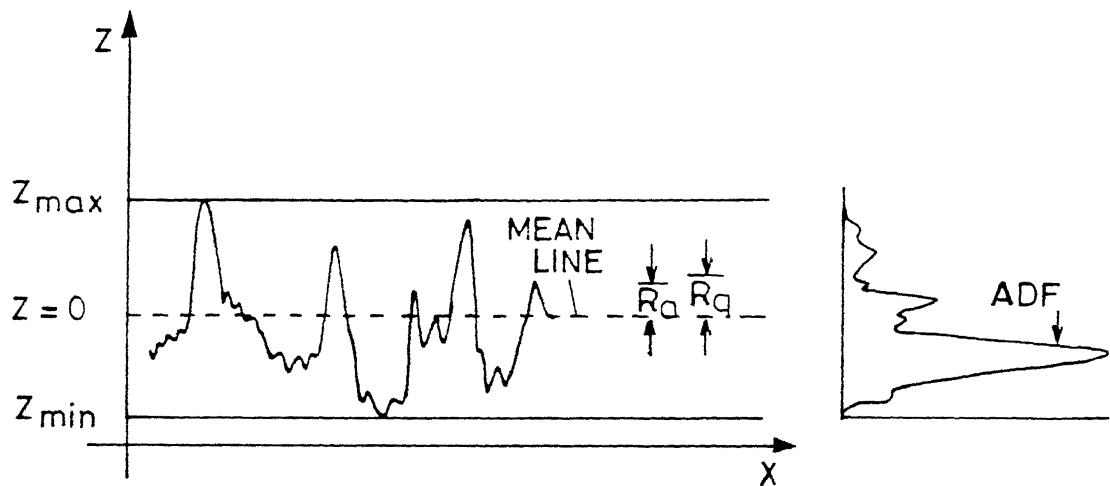
FIG. 1.5 AMPLITUDE DENSITY FUNCTION.

AVERAGE SLOPE (S_a) and RMS SLOPE (R_q) are hybrid parameters which combine both the amplitude and wavelength properties of surface. For a continuous surface profile they can be defined as

$$S_a = \frac{1}{L} \int_o^L |df/dx| dx$$

$$S_q = (\frac{1}{L} \int_o^L (df/dx)^2 dx)^{1/2}$$

Typical value of R_a for engineering surfaces range from 0.1 μm to 10μm and typical wavelength range from 5 μm to 800 μm. Surface structures with wavelengths greater than 800 μm are classified as waviness. The R_a value produced by various processes are shown in Fig.1.6.

1.4 LITERATURE SURVEY

Measuring surface roughness by scattering of light from rough surface have been studied over years and empirical relations derived [2,3].However no exact method is available which can cover the whole range of engineering surfaces. Stylus method still remains the conventional method for surface roughness measurement. Various techniques for the measurement of surface finish can be broadly classified into two groups [4] namely,

1.4.1 Profiling technique: In which the topographic information is derived from a point-by-point scan of surface height Z as a function of distance x along a straight line on the surface. The resulting profile is analysed by either analogor digital methods to derive roughness parameters [5]. Interferometry and stylus method come under this technique.
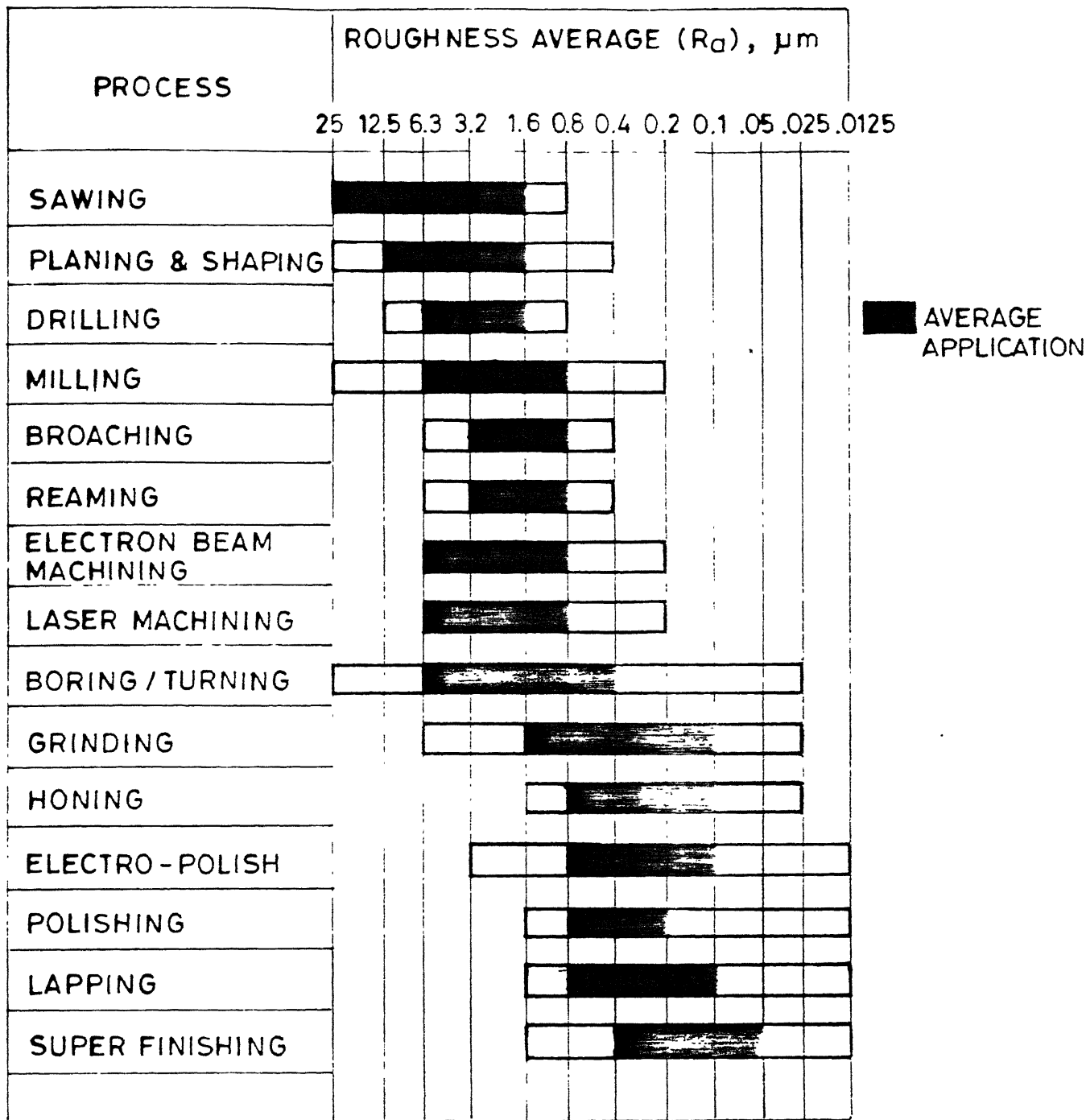
FIG.1.6 SURFACE ROUGHNESS PRODUCED BY COMMON
PRODUCTION METHODS.

1.4.1a   Stylus Method: Is the most widely used and is the oldest method of measuring surface profiles. It applies same principle as that of gramophone, where a sharp probe traverses a surface and transforms its minute irregularities into electrical signal.

1.1.4b   Interferometery: Is usually used to measure roughness of high-quality optical surfces by studying the fringe pattern prduced.

1.4.2   Parametric technique: The technique directly measures a parameter that represents some property of the surface topography averaged over the <u>illuminated</u> area. Methods like measurement of light reflected in *specular direction, total intensity of scattered light, the diffuseness of the angular scattering pattern, the speckle contrast and the polarization, to study the surface topography come under this category.

1.4.2a   Specular reflectance is the method in which the light intensity scattered in specular direction (I_s) is related to R_a or R_q value of the surface [6,7,8].

1.4.2b   Diffuseness of scattered light employs the ratio of intensities in specular direction to some off-specular direction and empirical relations to measure surface rougness derived for that particular surface only [2,9].

1.4.2c   Speckle contrast: When a rough surface is illuminated by partially coherent light, the reflected beam consists in part of random patterns of bright and dark regions known as speckle.   The

---

* Specular direction is the direction at an angle of reflectance equal to angle of incidence.

spatial pattern and contrast of speckle depend upon optical system, coherence condition of illumination and surface roughness of the scattering surface and is used to study surface microtopography.

1.4.2d **Ellipsometery** employes the measurement of change in the polarization of incident polarized light, which depends upon the composition of surface, surface structure, temperature, strain and surface roughness.

1.4.2e **Angular distribution (AD)**: By measuring the distribution of scattered light in space around the scattering region various parameters related to roughness amplitude as well as roughness wavelength are calculated. The kind of surface information that may be obtained from AD depends upon the roughness and spatial wavelength of rough surface [4,10,11, 12].

All the above methods described in parametric technique are still in experimental stage. Although much work has been done by many researchers with positive results. Table 1.1 gives the summary of optical techniques for surface roughness measurement as taken from [4].

1.4.3 **Existing theories:** The relationship between scattering and surface topography is complicated and according to our survey no exact theory is available. However, full vector electromagnetic theories are available in two opposite extremes [11] namely when vertical scale of roughness is much less than the wavelength of incident light and secondly when roughness amplitude

TABLE 1.1

SUMMARY OF OPTICAL TECHNIQUES FOR SURFACE ROUGHNESS MEASUREMENT

Technique	Quantitative? Capable of absolute measurements?	Can measure amplitude(A) & wavelength(W) parameters?	Speed (number of detector readings)	Horizontal resolution	Approximate vertical resolution μm	Vertical range of R_a, μm	Surface wavelength range, μm	Limits of vibration[+]	Can study isotropic or anisotropic surfaces?	Can study inner surfaces of parts?	Working devices existing?
Parametric											
Specular Reflectance	For $R_q < \lambda$	A	2	~1mm	≲0.001	~1	0.6–100	0.1D*	Yes	Yes	Yes
tis	For $R_q << \lambda$	A	2	~1mm	≲0.001	0.1	0.6–100	0.1D*	Yes	No	Yes
Diffuseness	Not yet	A	2	~1mm	~0.01	10	0.6–100	0.1D*	Yes	Yes	Yes
ad	For $R_q << \lambda$	AW	10–100	~1mm	≲0.001	>1	0.6–100	0.1D*	Yes	Yes	Yes
Laser Speckle Contrast	$R_q < 0.1\lambda$	A	100	~10λ	~10% of range	0.1	0.6–100	4λ/a³	Yes	+Q	No
Polychromatic Speckle Contrast	$\lambda/2 < R_q < 2l_c$	A	100	~1mm	~10% of range	2–5	0.6–100	4λ/a³	Yes	Q	No
Speckle Correlation	$\lambda < R_q < 10\lambda$	A	10	~1mm	~10% of range	1–30	0.6–100	4λ/a³	Yes	Q	No
Ellipsometry	Not yet	–	2	~1mm	<0.001	~1	?	?	Yes	Q	No
Profiling											
Interferometry	Yes	AW	1000	2 μm	≲0.001	<1	1–500	Limited by the desired resolution	Yes	No	Yes

[+] D* is the diameter of the detector aperture
‡ Q — questionable

is much greater than the wavelength of incident light. The precise condition for validity of smooth surface is given by [11,13]

$$(k_a \cos^2\theta_1)^2 \ll 1$$

where k = propagation vector = $2\Pi/\lambda$

λ = 6328.193A$^{\circ}$ for He-Ne Laser

a = vertical amplitude of roughness

θ_1 = angle of incidence

→ $a \ll 0.02$ A$^{\circ}$ for He-Ne laser

In this limit the scattering spectrum is given by

$$\frac{1}{I_1}\left(\frac{dI}{d\omega}\right) = 4k^4\cos\theta_1\cos^2\theta_s \times Q \times w(p,q)$$

where w(p,q) = psd of surface rughness evaluated at spatial wave numbers p and q.

and $$w(p,q) = \frac{1}{A} \left| \frac{1}{2\Pi} \int dx \int dy \, e^{i(px+qy)} Z(x,y) \right|^2$$

where $Z(x,y)$ = two dimensional surface profile

A = area of illuminated surface

Q = factor depending upon surface material and and polarization of incident light

θ_s = scattering angle w.r.t. θ_1

Hence the AD is direct fourier transform of surface profile $Z(x,y)$.

While in the case of rough surfaces the scattering comes from surface facets. In this case the scattering spectrum is given by

$$\frac{1}{I_i} \left(\frac{dI}{d\omega}\right)_s = \frac{(1+m_x^2 + m_y^2)^2}{4\cos\theta_i} \times R \times \rho(m_x, m_y)$$

where

I_i = input intensity

$d\omega$ = infinitesimally small solid angle into which

light is scatter at θ_s

m_x and m_y are x,y components of surface slopes.

$\rho(m_x, m_y)$ is the joint surface slope probability

distribution. Hence in this case the AD directly gives the probability distribution of slopes.

In our present work however ,effort is done to measure the surface roughenss by measuring AD of scattered laser light, considering the AD as diffraction pattern obtained by a periodic diffraction grating of constant amplitude and wavelength as is explained in chapter 2. Chapter 3 describes the experimental set-up, while in chapter 4 and chapter 5 experimental results and conclusion are given. The theory on which the experimental set-up is based is given in next chapter.

CHAPTER 2

THEORETICAL ANALYSIS

A rough surface scatters the collimated beam of laser light into an AD (Fig.2.1) according to the laws of physical optics. The Intensity and pattern of AD depends upon roughness heights, spatial wavelength, wavelength of light and angle of incidence with which the light interacts with the rough surface. This AD can be seen as the diffraction pattern obtained by a periodic diffraction grating of constant amplitude and wavelength.

2.1 GENERAL SOLUTION (By Peter Beckmann [6])

Assuming that S be a continuous rough surface in 2-dimensions given by $S = Z(x,y)$, (Fig.2.2) and a collimated beam of He-Ne laser be incident on it at an angle of incidence θ_1 w.r.t normal. The light is scattered in all directions according to the laws of physical optics. Let point of observation P be placed at an arbitrary position θ_2 w.r.t normal then,

(1) Using cartesian coordinates (x,y,z) with origin at O, and unit vectors $\vec{x}_o, \vec{y}_o, \vec{z}_o$.

(2) Let the rough surface be given by the function $S = Z(x,y)$, and the mean level of the surface is plane $Z = 0$.

(3) The incident field is E_1 and the scattered field is E_2. E_1 is assumed to be linearly polarized. Assuming E_1 to be a plane wave of unit amplitude.

$$E_1 = e^{i\vec{k}_1 \cdot \vec{r} - i\omega t}$$
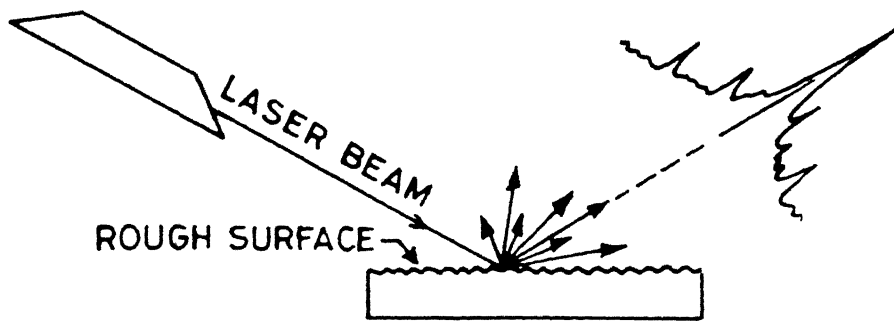
FIG. 2.1 ANGULAR DISTRIBUTION (AD) OF LIGHT
        SCATTERED BY A ROUGH SURFACE.
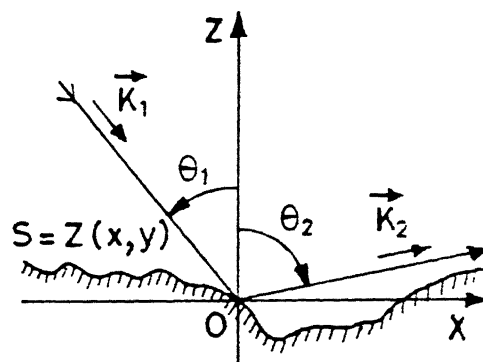
FIG. 2.2 BASIC NOTATION

where $\vec{k}_1 = \frac{2\Pi}{\lambda} \frac{\vec{k}_1}{|k|}$ = Propagation vector

$\vec{r}$ = radius vector = $x\vec{x}_o + x\vec{y}_o + z\vec{z}_o$

and in particular, for points on the surface S:

$r = x\vec{x}_o + y\vec{y}_o + Z(x,y)\vec{z}_o$

The angle of incidence, included between the direction of propagation of E_1 and Z axis, is denoted by θ_1; The scattering angle included between Z_o and $\vec{k}_2$ is denoted by θ_2. Where

$\vec{k}_2 \cong \vec{k}_1 = k = 2\Pi/\lambda$

θ_1 and θ_2 are measured in opposite senses from the +ve Z-axis. Since we are using coherent beam of light, hence the factor $e^{i\omega t}$ of $E_1 = Ae^{i\vec{k}_1.\vec{r}-i\omega t}$ can be suppressed.

Now assuming origin at O, and point of incidence at S = Z(x) be a one dimensional profile (since in the present work roughness variation along y is assumed to be negligible).

Let P be the point of observation and let R' be the distance from P to a point (x,Z(x)) on the surface S. The scattered field E_2 at P is given Helmholtz Integral (Fig.2.3)

$$E_2(P) = \frac{1}{4\Pi} \iint_S (E \frac{\partial \psi}{\partial n} - \psi \frac{\partial E}{\partial n}) \, ds \qquad (1)$$

where $\psi = \frac{e^{ik_2 R'}}{R'}$ \qquad (2)

In order to deal with plane scattered waves, rather than spherical ones, let R' → ∞ i.e. removing P to the Fraunhofer zone of

diffraction. Then

$$k_2 R' = k_2 R_0 - \vec{k}_2 \cdot \vec{r} \tag{3}$$

where R_0 = distance of P from the origon, so that

$$\psi = \frac{e^{ik_2 R_0 - i\vec{k}_2 \cdot \vec{r}}}{R_0} \tag{4}$$

E and $\frac{\partial E}{\partial n}$ are the field and its normal derivative on S = Z(x). And

in the present case we shall assume the field E_S at any point of

the surface to be field at the tagent plane on that surface.

Within the assumption we have

$$(E)_S = (1+R)E_1 \tag{5}$$

where 1 is due to incident field and R is due to reflected field

and $\qquad (\frac{\partial E}{\partial n})_S = (1-R) E_1 \vec{k}_1 \cdot \vec{n} \tag{6}$

n = is the normal to the surface at the considered point and R is

the reflection coefficient of the smooth plane.

R = f(angle of incidence, electrical properties,

polarization)

$\qquad$ Eq. (6) follows from

$\qquad (H)_S = (1-R) H_1$ and

$$\nabla \times E = -\frac{\partial B}{\partial t} = -\mu \frac{\partial H}{\partial t}$$

$$\nu = \theta_1 - \beta = \theta_1 - \tan^{-1} \frac{\partial Z(x)}{\partial x}$$

and $\qquad \frac{\partial \psi}{\partial n} = (\nabla \psi \cdot n) = (\frac{\partial \psi}{\partial R'}) \cdot \vec{n} \tag{7}$

Substituting 4,5,6 and 7 in (1) we get

$$E_2 = \frac{i e^{ikR_0}}{4\pi R_0} \int_S (R\vec{\nabla} - \vec{P}) \cdot \vec{n} \, e^{i\vec{\nabla} \cdot \vec{r}} \, ds \tag{8}$$
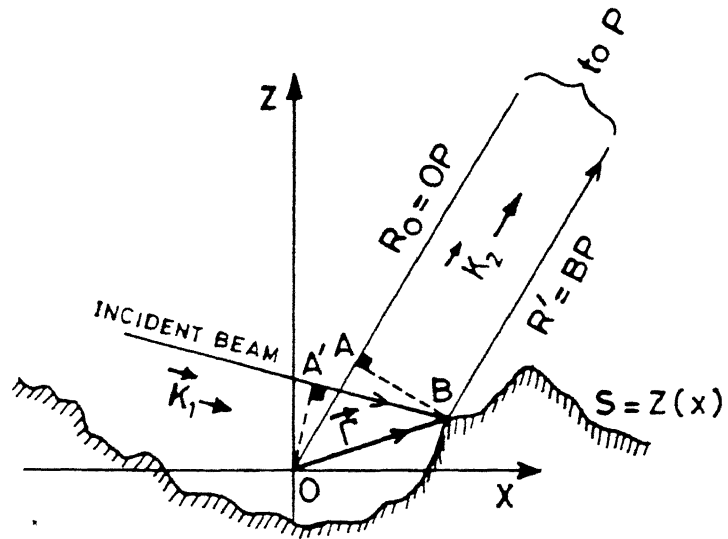
FIG. 2.3 DERIVATION OF EQUATION NO. (3)
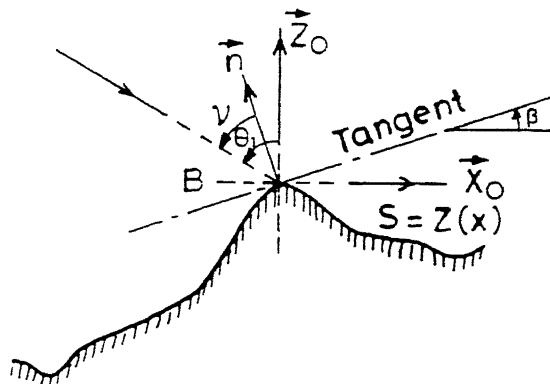
FIG. 2.4 LOCAL SCATTERING GEOMETRY

where $\qquad \vec{V} = \vec{k}_1 - \vec{k}_2$ (9)

$$\vec{P} = \vec{k}_1 + \vec{k}_2 \qquad (10)$$

Resolving (9) and (10) into their cartesian components, we have

$$\vec{V} = k(\sin\theta_1 + \sin\theta_2)\vec{x}_0 - k(\cos\theta_1 + \cos\theta_2)\vec{z}_0 \qquad (11)$$

$$= V_x\vec{x}_0 + V_z\vec{z}_0$$

$$\vec{P} = k(\sin\theta_1 + \sin\theta_2)\vec{x}_0 + k(\cos\theta_1 - \cos\theta_2)\vec{z}_0 \qquad (12)$$

$$\vec{n} = -\vec{x}_0\sin\beta + \vec{z}_0\cos\beta \qquad (13)$$

$$\vec{r} = x\vec{x}_0 + Z(x)\vec{z}_0 \qquad (14)$$

$$ds = \sec\beta.dx; \quad \tan\beta = \frac{\partial Z(x)}{\partial x} \qquad (15)$$

For a surface extending from $x = 0$ to $x = 2L$, E_2 in scalar form can be written as

$$E_2 = \frac{ie^{ikR_0}}{4\pi R_0} \int_0^{2L} (a\frac{\partial Z(x)}{\partial x} - b)e^{iV_x x + iV_z Z(x)} \quad dx \qquad (16)$$

where $\qquad a = (1-R)\sin\theta_1 + (1+R)\sin\theta_2$ (17)

$$b = (1+R)\cos\theta_1 - (1-R)\cos\theta_2) \qquad (18)$$

To get rid of factor in front of integral in eq.no. (16) we normalize the expression by introducing the scattering coefficient

$$\rho = \frac{E_2}{E_{20}} \qquad (19)$$

E_{20} = field reflected in specular direction ($\theta_2 = \theta_1$) by a smooth, perfectly conducting plane of the same dimensions under the same angle of incidence and at the same distance

$$\rightarrow V_x = 0 \; ; \; Z(x) = 0, \; \frac{\partial Z(x)}{\partial x} = 0 \text{ and from } (16) \& (18)$$

We find that

$$E_{20} = \frac{ike^{ikR_o}}{\pi R_o} \; L\cos\theta_1 \qquad (20)$$

Hence from (16) and (20) we have

$$\rho = \text{scattering coefficient}$$

$$\rho = \frac{1}{4L\cos\theta_1} \int_0^{2L} (a\frac{\partial Z(x)}{\partial x} - b)e^{iV_x x + iV_z Z(x)} \, dx \qquad (21)$$

The integral (21) is easily integrated if a and b are assumed to be constants. One way of achieving this is to average R over the surface, making a and b independent of x (since a and b depend upon R and V). Or the other is assuming Y = CONDUCTIVITY $\rightarrow \infty$ i.e. We have a perfectly conducting plane. Defining suffix (+) for vertical polarisation and (-) for horizontal polarisation, i.e. for

VERTICAL POLARISATION $R^+ = +1$ for E_1, E_2 in plane of incidence (22)

HORIZONTAL " $R^- = -1$ for $E_1, E_2 \perp$ to plane of incidence (23)

Removing the brackets of (21) and solving the intergal as product of two functions $a\frac{\partial Z(x)}{\partial x} e^{iV_z Z(x)}$ and $e^{iV_x x}$ and using the formula that

$$\int f'(x)e^{af(x)} \, dx = \frac{e^{af(x)}}{a}$$

where $\qquad f'(x) = \frac{\partial f(x)}{\partial x}$

we get

$$\rho = \frac{1}{4L\cos\theta_1}\left[(b + \frac{aV_x}{V_z}) \int_0^{2L} e^{i\vec{V}.\vec{r}} \, dx - \frac{ia}{V_z} \, e^{i\vec{V}.\vec{r}}\Big|_0^{2L} \right] \qquad (24)$$

Substituting (22) and (23) in (17) and (18) we have

$$a^+ = 2\sin\theta_2 \qquad b^+ = 2\cos\theta_2$$
$$\left. a^- = 2\sin\theta_1 \qquad b^- = 2\cos\theta_1 \right] \qquad (25)$$

Substituting these values in (24) we have

$$\rho^{\pm}(\theta_1,\theta_2) = \pm\,\sec\theta_1\,\frac{1+\cos(\theta_1+\theta_2)}{\cos\theta_1+\cos\theta_2}\times\frac{1}{2L}\int_0^{2L} e^{i\vec{V}.\vec{r}}\,dx + \frac{e^{\pm}(L)}{2L} \qquad (26)$$

where

$$\rho^{\pm}(L) = \frac{i\,\sec\theta_1\,\sin\theta^{\pm}}{k(\cos\theta_1+\cos\theta_2)}\,e^{i\vec{V}.\vec{r}}\Big|_0^{2L} \qquad (27)$$

$$\text{with } \theta^+ = \theta_2$$
$$\theta^- = \theta_1$$

$\vec{V}.\vec{r}$ is given explicitly as

$$\vec{V}.\vec{r} = \frac{2\pi}{\lambda}\,([\sin\theta_1-\sin\theta_2]x - [\cos\theta_1+\cos\theta_2]Z(x) \qquad (28)$$

Now for the surface such that $L \gg \lambda$, II term of (26) can easily be shown to be negligible as compared to (I) term . Hence (26) reduces to simple formula

$$\boxed{\rho = \frac{F_2}{2L}\int_0^{2L} e^{i\vec{V}.\vec{r}}\,dx} \qquad \text{for vertical polarization}$$

$$\qquad (28)$$

where $F_2(\theta_1,\theta_2) = \left(\dfrac{1+\cos(\theta_1+\theta_2)}{\cos\theta_1+\cos\theta_2}\right)\sec\theta_1$ \qquad (29)

2.2 GENERAL KIRCHOFF SOLUTION OF THE FIELD SCATTERED BY A PERFECTLY CONDUCTING PERIODIC SURFACE

Assuming the surface S to be rough in one dimension only i.e. along x. Since $Z(x)$ is periodic of period Λ

$$\Rightarrow Z(x) = Z(x+\Lambda) \tag{1}$$

Λ = wavelength of the Roughness

The integral (26) of previous section will be periodic with period Λ if

$$V_x \Lambda = 2\pi m \text{ (where } m = 0, \pm 1, \pm 2, \ldots = \text{integer)} \tag{2}$$

Since by (11) of last section

$$V_x = \frac{2\pi}{\lambda} (\sin\theta_1 - \sin\theta_2) \tag{3}$$

We may write (2) as $\sin\theta_{2m} = \sin\theta_1 - \dfrac{m\lambda}{\Lambda}$ (4)

which is a well known grating equation

Let $\quad \dfrac{2L}{\Lambda} = n+n_1 \quad$ where n = integer

n_1 = pure fraction $(0 \leq n_1 < 1)$

since $\int e^{i v \cdot r} dx$ is periodic with period Λ we may write

$$\int_0^{2L} e^{i\vec{V}\cdot\vec{r}} dx = n\int_0^{\Lambda} + \int_0^{n_1\Lambda} = \frac{2L}{\Lambda} \int_0^{\Lambda} + \int_0^{n_1\Lambda} - n_1 \int_0^{\Lambda} \tag{5}$$

Substituting (2) in (27) of previous chapter we have

$$e(L) = e(\frac{2\pi m n_1}{V_x}) \tag{6}$$

Substituting (5) and (6) in (26) Section 2.1, we have for perfectly conducting, 1-dimensional periodic surface

$$\rho^{\pm}(\theta_1,\theta_2) = \pm \sec\theta_1 \frac{1+\cos(\theta_1+\theta_2)}{\cos\theta_1 + \cos\theta_2} \quad \frac{1}{\Lambda} \int_0^{\Lambda} e^{i\vec{V}.\vec{r}}dx + \frac{c(n_1)}{2L}$$

$$(7)$$

$$c(n_1) = F_2(\theta_1,\theta_2)[\int_0^{n_1\Lambda} e^{i\vec{V}.\vec{r}}dx - n_1 \int_0^{\Lambda} d^{i\vec{V}.\vec{r}}dx] + e(2\pi m n_1/V_x)$$

$$(8)$$

Third term of (8) is the correction term or "edge effect" which vanishes as $n_1 \to 0$ i.e. when $\frac{2L}{\Lambda}$ integral ; In any case (8) is shown to be negligible when $L >> \Lambda$. Comparing (4) with the normal grating equation. If we calculate the path difference for the A&B rays such that they are in phase i.e. P.D. = $2\pi m$(Fig. 2.5) We get eq.no.(4). Hence θ_{2m} correspond to the local maxima of scattered light from the rough surface. Returning to equation no.(4) we see that total no. of possible modes is limited by condition $|\sin\theta_{2m}| \leq 1$. The mode $m = 0$ is the specular mode and $m = \pm 1$ lie on either side of specular mode(Fig.2.6) until $\theta_2 m = \pm \pi/2$. (Mode = light scattered in the direction of maxima i.e. point at which constructive superposition of waves takes place)

Now integral (7) gives the coefficient in the direction of maxima only. Hence If we want to find out the light scattered in (any other) direction other than θ_{2m} we then return to general solution (26) of last section and neglecting the "edge effect" term we have :

$\frac{2L}{\Lambda} = n$, $n_1 = 0$. Divide 2L into n strips each extending from $x = j\Lambda$ to $x = (j+1)\Lambda$ where $j = 0$, $(n-1)$

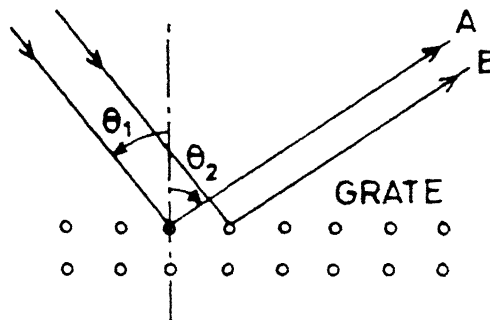$\Rightarrow n$ = no. of scatterers = no. of periods present. Hence
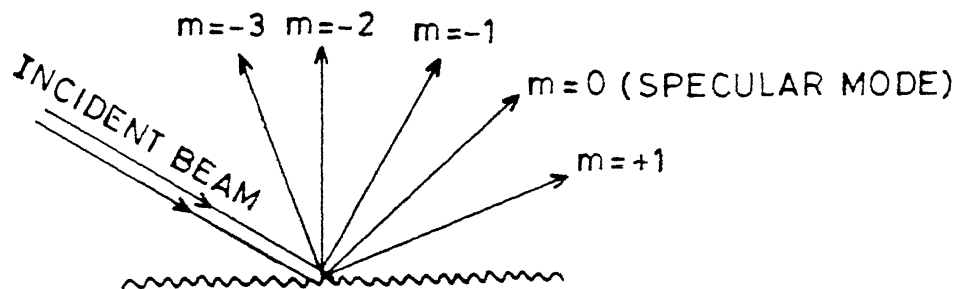
FIG. 2.5 DERIVATION OF GRATING EQUATION

FIG. 2.6 DIRECTIONS OF SCATTERED MODES BY
PERIODIC SURFACE

$$\frac{1}{2L} \int_0^{2L} e^{i\vec{V}.\vec{r}} dx = \frac{1}{n\Lambda} \sum_{j=0}^{n-1} \int_{j\Lambda}^{(j+1)\Lambda} e^{iV_x x + iV_z Z(x)} dx \qquad (9)$$

Since we are in fraunhofer zone, each scatterer acts in the same manner

Now put $V_x \Lambda = 2\pi p$ (p = any no./not necessarily an integer)

(10)

We have $P = \frac{\Lambda}{\lambda} (\sin\theta_1 - \sin\theta_2)$ (11)

We have from (9)

$$\frac{1}{2L} \int_0^{2L} e^{i\vec{V}.\vec{r}} dx = \frac{1}{n} \sum_{j=0}^{n-1} e^{i2\pi p j} \frac{1}{\Lambda} \int_0^{\Lambda^{\cdot}} e^{i\vec{V}.\vec{r}} dx \qquad (12)$$

Now (12) differ from (7) by the factor

$$W = \frac{1}{n} \sum_{j=0}^{n-1} e^{i2\pi p j} = \frac{\sin (p\pi n)}{n \sin (p\pi)} \qquad (13)$$

Hence the general solution for perfectly conducting periodic surface as seen at fraunhofer zone for any scattering angle θ_2 =

$$\rho^{\pm}(\theta_1,\theta_2) = \pm \frac{\sin(np\pi)}{n\sin(p\pi)} \sec\theta_1 \frac{1+\cos\theta_1+\theta_2)}{\cos \theta_1+\cos\theta_2} \frac{1}{\Lambda} \int_0^{\Lambda} e^{i\vec{V}.\vec{r}} dx + O(n_1/n)$$

(14)

$O(n_1/n)$ = correction term which vanishes for $2L/\Lambda$ = integral

2.2.1 APPLICATION TO SPECIFIC PERIODIC PROFILES

Now in our case the specimens are made on milling m/c giving high periodicity and the likely profile is to be of triangular nature. Hence solving (14) section 2.2 for a triangular profile and extending theory for more practical case.

Assu ming a triangular (Δ profile) of the shown characteristics in figure 2.7. Where

$$2h = \text{height}$$

$$\Lambda = \Lambda_1 + \Lambda_2 \quad \text{wavelength/period}$$

$$\phi_1, \phi_2 = \text{Angles depending upon tool geometry}$$

$$\phi_1 = 90^\circ - \text{effective side cutting edge angle}$$

$$\phi_2 = \text{effective end cutting edge angle (Fig.4.9)}$$

Now cordinates of $O \leftrightarrow (0,0)$; $A \leftrightarrow (\Lambda_1, 2h)$; $B \leftrightarrow (\Lambda, 0)$

Now

$$Z(x) = \begin{cases} OA = \dfrac{2h}{\Lambda_1} x; & 0 \leq x \leq \Lambda_1 \\[2mm] AB = \dfrac{2h}{\Lambda_2}(\Lambda - x); & \Lambda_1 \leq x \leq \Lambda \end{cases}$$

and $I = \displaystyle\int_0^\Lambda e^{iV_x x + iV_z Z(x)} dx$ of $(14) = \displaystyle\underbrace{\int_0^{\Lambda_1} e^{iV_x x + iV_z Z(x)} dx}_{I_1} + \underbrace{\int_{\Lambda_1}^\Lambda e^{iV_x x + iV_z Z(x)} dx}_{I_2}$

$$I_1 = \int_0^{\Lambda_1} e^{i\vec{V}\cdot\vec{r}} dx = \int_0^{\Lambda_1} e^{iV_x x + \frac{i2hV_z x}{\Lambda_1}} dx = \int_0^{\Lambda_1} e^{i(V_x + \frac{2hV_z}{\Lambda_1})x} dx$$

$$= \left(\frac{2}{C_1} \sin C_1 \frac{\Lambda_1}{2}\right) * e^{iC_1 \frac{\Lambda_1}{2}} = R_1 e^{i\mu_1} \quad (15)$$

where $C_1 = V_x + \dfrac{2hV_z}{\Lambda_1}$ \hfill (15a)

$$R_1 = \frac{2}{C_1} \sin\left(C_1 \frac{\Lambda_1}{2}\right) \qquad\qquad (15b)$$

$$\mu_1 = C_1 \frac{\Lambda_1}{2} \qquad\qquad (15c)$$

$$I_2 = \int_{\Lambda_1}^{\Lambda} e^{iV_x x + iV_z \frac{2h}{\Lambda_1} \Lambda - iV_z \frac{2hx}{\Lambda_2}}$$

$$= e^{iV_z \frac{2\Lambda h}{\Lambda_2}} \int_{\Lambda_1}^{\Lambda} e^{i(V_x - \frac{2hV}{\Lambda_2}z)x} \, dx = R_2 e^{i\mu_2} \qquad (16)$$

$$R_2 = \frac{2}{C_2} \sin(C_2 \frac{\Lambda_2}{2}) \qquad (16a)$$

$$\mu_2 = 2hV_z \frac{\Lambda}{\Lambda_2} + C_2\Lambda_1 + (C_2\Lambda_2/2) \qquad (16b)$$

$$C_2 = V_x - 2V_z \frac{h}{\Lambda_2} \qquad (16c)$$

$$I = I_1 + I_2 = R_1 e^{i\mu_1} + R_2 e^{i\mu_2} = Re^{i\mu} \qquad (17)$$

$$\text{Where} \qquad R^2 = R_1^2 + R_2^2 + 2R_1R_2 \cos(\mu_1 - \mu_2) \qquad (17a)$$

$$\& \qquad \tan\mu = \frac{R_1 \sin\mu_1 + R_2 \sin\mu_2}{R_1 \cos\mu_2 + R_2 \cos\mu_2} \qquad (17b)$$

2.2.1a ` I CONSIDERATION

Assuming detector is at Fraunhofer Zone put (17) in (14) to get general distribution of light amplitude at Fraunhofer zone

$$\rho = (W*F*\frac{Re^{i\mu}}{\Lambda}) \qquad (18)$$

where $W = \frac{\sin(np\pi)}{n\sin(p\pi)}$; $F = \sec\theta_1 \frac{1 + \cos(\theta_1 + \theta_2)}{\cos\theta_1 + \cos\theta_2}$; R & μ are given by

(17a) and (17b) of section 2.2.1 respectively

2.2.1b   II CONSIDERATION

Now, in practice it is not possible to put the detector in the Fraunhofer Zone to measure angular distribution. Hence for a periodic surface, the total field scattered into a certain
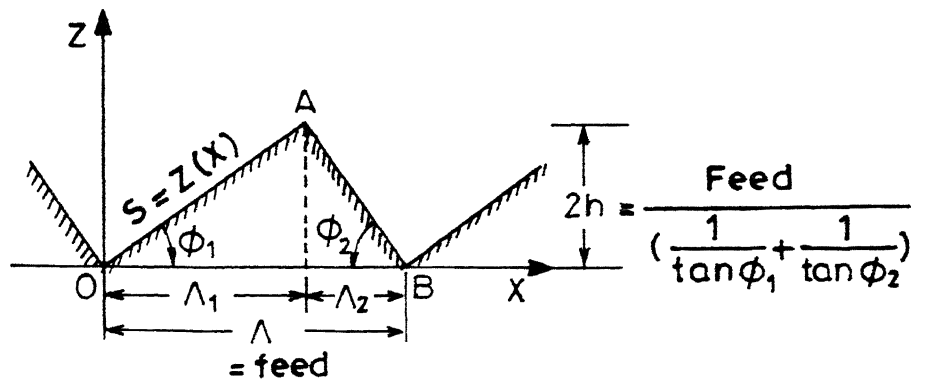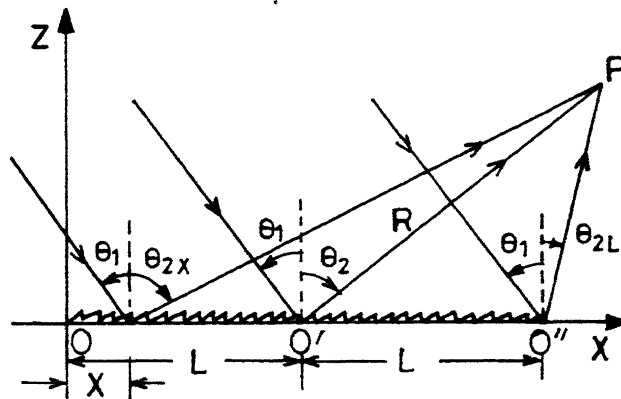
FIG. 2.7 PROFILE SPECIFICATIONS.

$$2h = \frac{Feed}{(\frac{1}{\tan\phi_1} + \frac{1}{\tan\phi_2})}$$

FIG. 2.8 FIELD AT ANY POINT P IN FRESNEL ZONE
IS SUM OF AMPLITUDES SCATTERED BY
DIFFERENT WAVE PERIODS.

direction is given by adding the contributions of each period to that direction (Fig.2.8). Now since in this kind of situation θ_2 has a weak dependence x. Hence V_x, V_z,C_1,C_2 vary along the x hence we return to general solution (21) of last chapter and assuming θ_2 = constant for x = jΛ to x = (j+1)Λ for j = 0,(n-1) we have `a' and `b' of last section 2.1 eq. (17) & eq.(18) also constant →

$$\rho = \frac{1}{4L\cos\theta} * \int_0^\Lambda (a \frac{\partial Z(x)}{\partial x} - b) \, e^{iV_x x + iV_z Z(x)} \, dx \qquad (19)$$

O'= Reference point & O'P = R´

$$\theta_{2x} = \tan^{-1} (\frac{x-L}{R\cos\theta_2} + \tan \theta_2) \qquad (20)$$

breaking (19) for each scatterer we have

$$\rho = \frac{1}{4L\cos\theta_1} * \left[\int_o^\Lambda (\ )dx + \int_\Lambda^{2\Lambda} (\ )dx + ...+ \int_{j\Lambda}^{(j+1)\Lambda} + ... \int_{(n-1)\Lambda}^{n\Lambda} (\ ) \, dx \right] \qquad (21)$$

taking j^{th} integral we have

$$\rho_j th = = \frac{1}{4L\cos\theta_1} * \int_{j\Lambda}^{(j+1)\Lambda} (a \frac{\partial Z(x)}{\partial x} - b) e^{iV_x x + iV_z Z(x)} \, dx \qquad (22)$$

Since a,b,V_x and V_z are i.e θ_2 is assumed to be constant between one wave period. Hence solving (22)

Just like (21) of previous chapter we have

$$\rho_j \text{th} = F_j * e^{i2\pi p} \int_0^\Lambda e^{iV_x x + iV_z Z(x)} \, dx \qquad (23)$$

$$F_j = \sec \theta_1 \frac{1 + \cos(\theta_1 + \theta_{2x})}{\cos\theta_1 + \cos\theta_2} * \frac{1}{2L} \qquad (24)$$

$$\text{and} \int_0^\Lambda e^{iV_x x + iV_z Z(x)} \, dx = R_j e^{i\mu_j}$$

since θ_2 varies for each j as x varies from

$$x = 0*j = 0 \text{ to } x = nj = 2L$$

Hence

$$\rho = \sum_{j=0}^{(n-1)} (F_j * e^{i2\pi pj} * R_j e^{i\mu_j}) \qquad (25)$$

Where R_j and μ_j are found from (17a) & (17b) by substituting θ_{2x} for θ_2; where θ_{2x} is given by (20).

2.3   OBSERVATIONS

Now the intensity scattered by a periodic rough surface in any direction θ_2 is given by eq. no. 18 section 2.2 as,

$$\rho = W * F * \frac{R}{\Lambda} e^{i\mu}$$

where R and μ are given by (17a) and (17b) of section 2.2., W by (13) section 2.2 and F by (29 section 2.1. Now for simplicity assuming that the point P of observation is placed in specular direction i.e. in that case $\theta_1 = \theta_2$ then observing the variations in specular intensity.

Now for $\theta_1 = \theta_2$ $\qquad\qquad\qquad\qquad$ (1)

$\rightarrow V_x = k (\sin \theta_1 - \sin\theta_2) = 0$ $\qquad\qquad$ (2)

and $P = \frac{\Lambda}{\lambda}(\sin\theta_1 - \sin\theta_2) = 0$ (3)

Hence $W = F = 1$ and putting (1)&(2) in (15a,b,c) and (16a,b,c) of section 2.2.1, we get

$$C_1 = -C_2 = 2V_z \frac{h}{\Lambda_2}$$

and $\mu_1 = \mu_2 = V_z h$

Hence $R^2 = (R_1 + R_2)^2 = {}^*\text{sinc}^2(V_z h)$ (4)

where $V_z = 2k\cos\theta_1 = 2k\cos\theta_2$

Hence intensity variation in specular direction is given by (4) i.e.

$$I_s = \text{Sinc}^2(V_z h) \quad\quad\quad (5)$$

2.3.1   Variation of θ_1 = angle of incidence

Now Re-writing   (4)

$$I_s = \text{sinc}^2(2kh\cos\theta_1) = f(\theta_1) \quad\quad (6)$$

Now as θ_1 goes on increasing the value I_s goes through a periodic function and at near grazing angle of incidence

$$\theta_1 \rightarrow 90^\circ$$

$$I_s \rightarrow 1 \quad\quad\quad\quad\quad (7)$$

Eq. (7) is a standard result i.e. at near grazing angle of incidence even the rough surfaces reflect specularly[**]. Hence (7) justifies our theory also. The variation of I_s is ploted theoretically for two surfaces having different values of h or in other words, different values of Ra (Fig. 2.9).

---

[*]$\text{Sincx} = \dfrac{\text{Sin } x}{x}$

[**]Phenomenon of Road glare

FIG. 2.9   SPECULAR INTENSITY FROM A FINE GRATIN
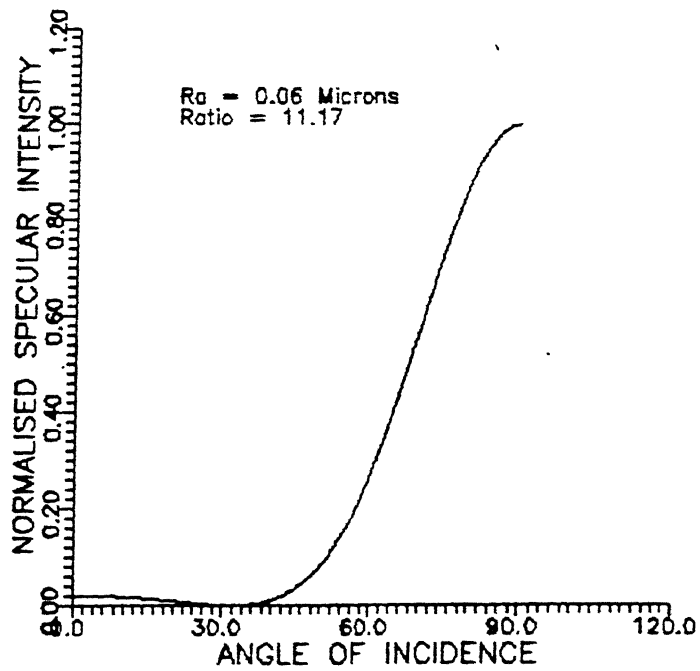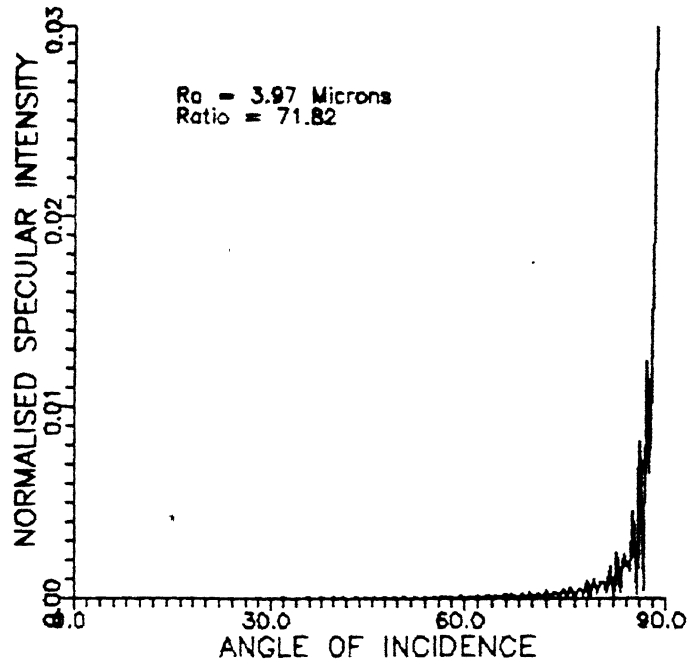
A look at the graphs show that for a smooth surface the light reflected in specular direction increases smoothly with increasing angle of incidence, while for a comparatively rough surface the variation is rather abrupt.

A look at eq. (4) shows that the <u>light reflected in specular direction is independent of the spatial wavelength of the roughness</u>. Hence it can be utilised as a strong tool to measure the Ra value of rough surfaces

2.3.2 **Variation of h :** Now if we keep θ_1 constant and try to see the effect on I_s by the variation of h i.e.. The roughness amplitude, we have

$$I_s = \text{sinc}^2(V_z h) \tag{8}$$

Hence as $h \rightarrow 0$ i.e. approaching a perfectly smooth surface

$$I_s \rightarrow 1 \tag{9}$$

Hence a perfectly smooth surface reflects all the incident light in specular direction which is logically true also. Hence Eq. (9) confirms that the theory is correct. Fig.(2.10) show the variation of specular intensity vs roughness amplitude for two angles of incidence. Figure shows that light scattered in specular direction goes on decreasing with increase in roughness of the surface.

2.3.3 **Theoretical Angular distribution (AD)** According to eq.(4) section 2.2.1 the scattering pattern consists of finite
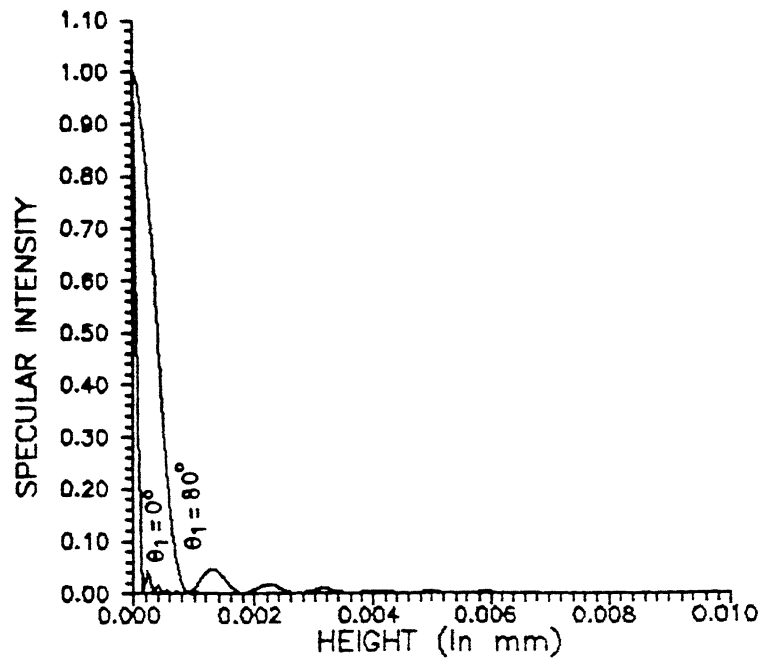
FIG. 2.10.   VARIATION OF SPECULAR INTENSITY
.WITH ROUGHNESS HEIGHT (h)

diffraction spots at discrete angles, when the scattering pattern
is obtained by perfectly conducting periodic surface and the no.
of diffraction spots depend upon the ratio :

$$r = \frac{\Lambda}{\lambda}$$ (10)

That is larger this ratio more the no. of scattered modes.
The no. is given by

$$N = 2r+1$$ (11)

And the intensity propagated in each mode is given by (25) section
2.2.1b and the angle at which a particular mode is propagated or a
diffraction spot is obtained is given by

$$\theta_{2m} = \sin^{-1} (\sin \theta_1 - \frac{m\lambda}{\Lambda})$$ (12)

m = +ve or -ve integer

m = 0 for specular mode

where max. and min. value of m is obtained by putting $\sin(\theta_{2m}) = +$
1 and -1 respectively

For example, for a surface having ratio [*] r = 11.58 the total no.
of scattered modes is
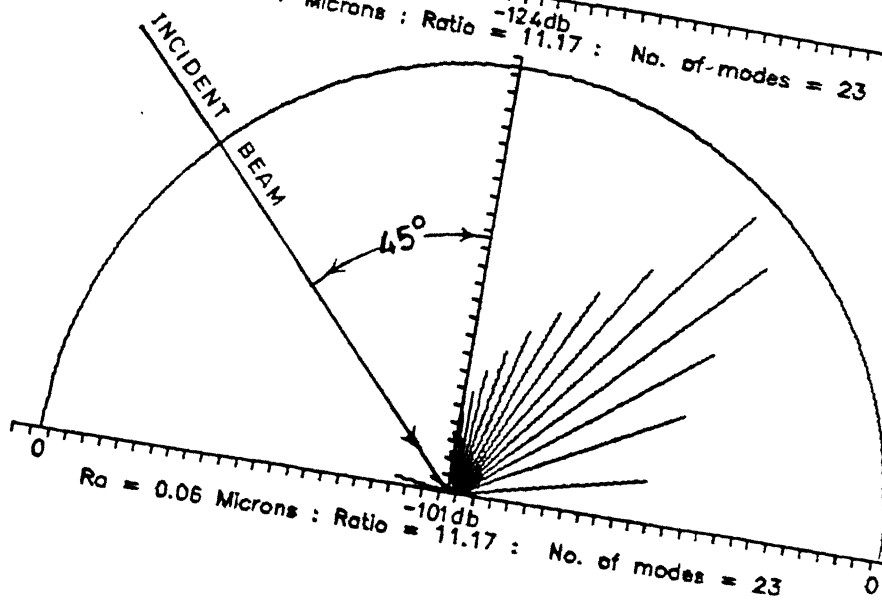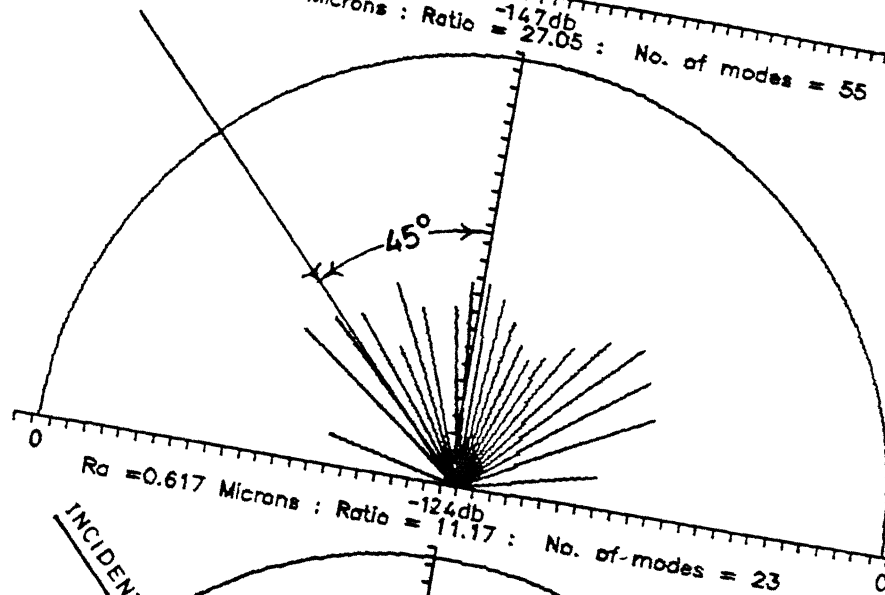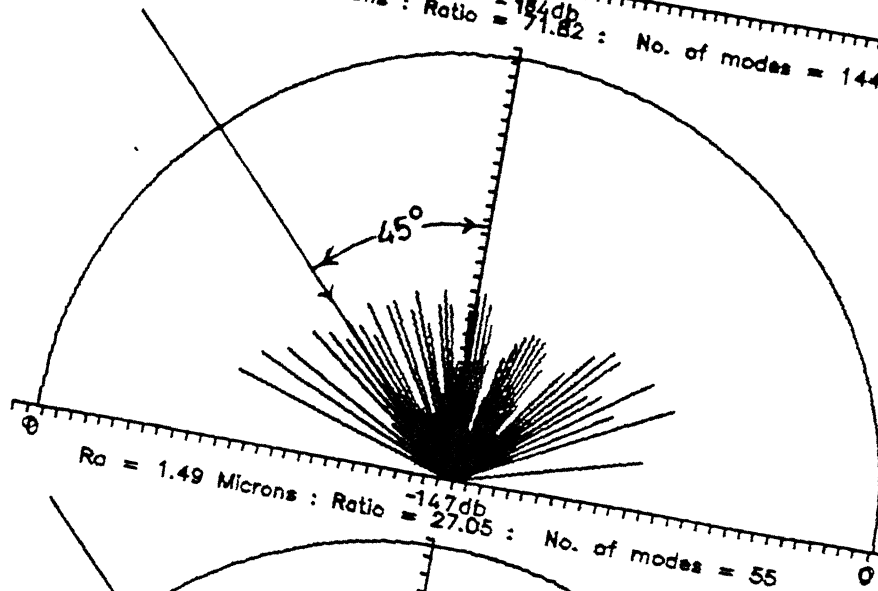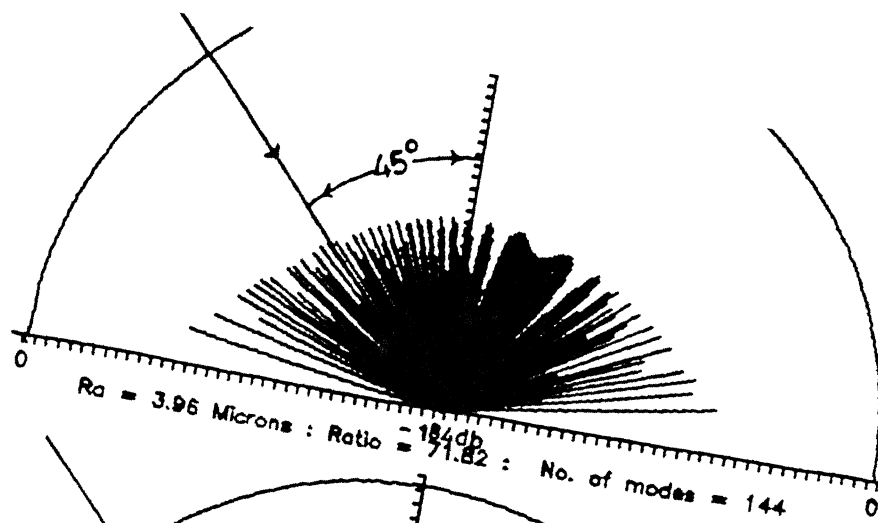
$$(2r+1) = 24.176$$

Since the fractional part has no significance hence

$$N = 24$$

Fig (2.11) shows the theoretical scattering pattern by a
triangular surface.

But according to [11] each surface is a superposition of both
random as well as periodic roughness. Hence the presence of

---

[*] = 11.58 corresponds to f = 22mm/min and R.P.M. = 3000 on milling n

Ra = 3.96 Microns : Ratio = $\frac{-184db}{71.82}$: No. of modes = 144

Ra = 1.49 Microns : Ratio = $\frac{-147db}{27.05}$: No. of modes = 55

Ra = 0.617 Microns : Ratio = $\frac{-124db}{11.17}$: No. of modes = 23

Ra = 0.06 Microns : Ratio = $\frac{-101db}{11.17}$: No. of modes = 23

45°

45°

45°

45°

INCIDENT BEAM

0

0

0

0

0

0

0

0

θs=Scattering angle w.r.t. angle of incidence θi = 0°
Ra = 0.025 Microns
Ratio = 11.588
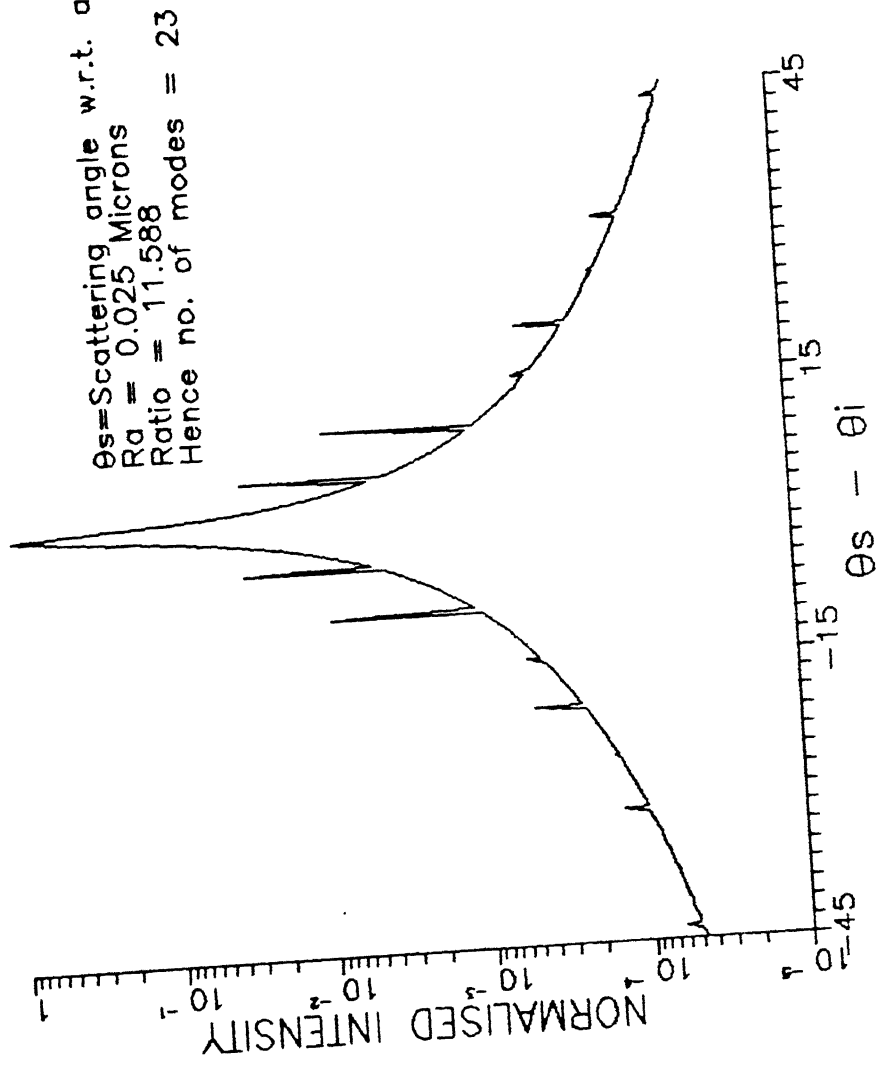Hence no. of modes = 23

NORMALISED INTENSITY

θs − θi

FIG. 2.12   THEORETICAL ÂD FOR A TRIANGULAR SURFACE

random one – dimensional component the total intensity falls off
as the second power of scattering angle away from the specular
direction. Hence the likely AD pattern to be obtained is shown in
figure 2.12.

2.3.4   Separation of modes :

Figure 2.13 shows the angular difference between two adjacent
modes for different values of spatial wave length Λ. The symmetry
of the plots   show that the modes are symmetrically placed
and the angular seperation is constant for in between modes.
Hence by measuring their angular difference it may be possible to
predict the spatial wavelength of the surface roughness . Table
(2.1) gives the theoretical separation between modes for different
values of spatial wavelength.

2.4 Conclusions :

By variation of different parameters the following
conclusions come forward

(a) Light reflected in specular direction goes on decreasing
with increase in surface roughness.

(b) At near grazing angle of incidence all the surfaces
tend to reflect specularly.

c) larger spatial wavelength components diffract light into
smaller angles while smaller spatial wavelength components
diffract light into larger angles

And a final conclusion that the roughness is a relative term when
compared with wavelength of incident light. Which is evident if
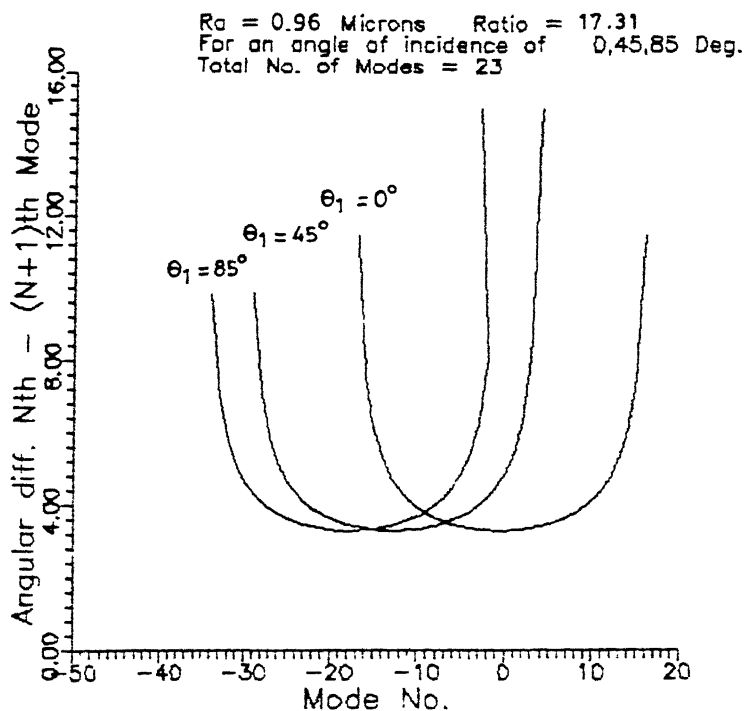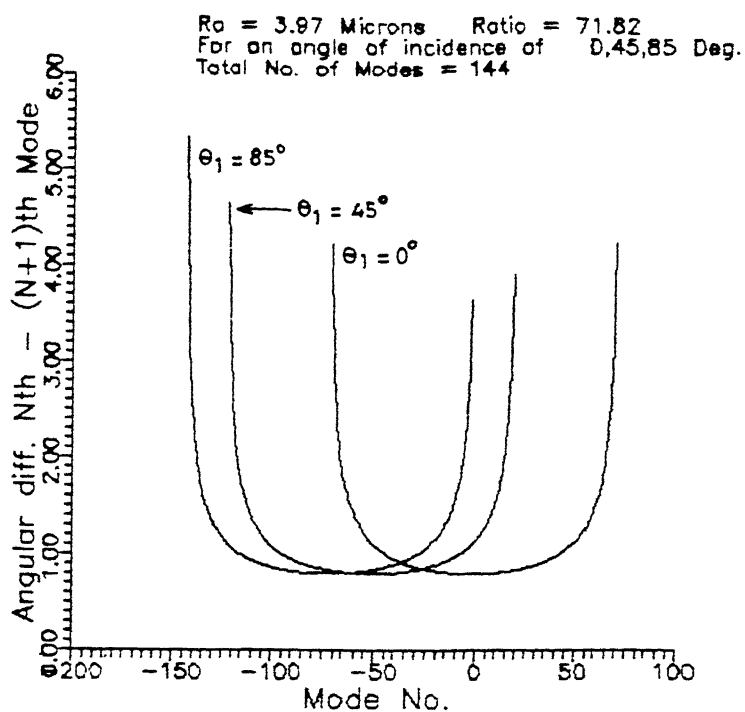we re-write (31) as

Ra = 3.97 Microns   Ratio = 71.82
For an angle of incidence of   0,45,85 Deg.
Total No. of Modes = 144

$\theta_1 = 85°$

$\theta_1 = 45°$

$\theta_1 = 0°$

Ra = 0.96 Microns   Ratio = 17.31
For an angle of incidence of   0,45,85 Deg.
Total No. of Modes = 23

$\theta_1 = 0°$

$\theta_1 = 45°$

$\theta_1 = 85°$

FIG. 2.13   THEORETICAL SEPARATION OF MODE

TABLE 2.1

MODE SPECIFICATIONS

Specimen No.	Ratio Λ/λ	Theoretical Separation of modes (deg.)	Theoretical No. of modes	Average Expt. spacing
FA-1	2522	0.022°	5045	2.2°
FA-2	1008.1	0.056°	2017	2.3°
FA-3	314	0.18°	629	2.67°
FA-4	77.43	0.74°	155	2.926°
MA-1	17.31	3.3°	35	
MA-2	34.63	1.6°	70	
MA-3	107.62	0.53°	216	
MA-4	68.19	0.84°	137	
MA-5	71.82	0.79°	144	3.15°
MA-6	27.05	2.1°	55	
MA-7	11.17	5.1°	23	
MA-8	17.464	3.28°	35	
MA-9	27.33	2.09°	55	
MA-10	17.31	3.3°	35	
MA-11	11.17	5.1°	23	

$$I_s = \text{sinc}^2(2*\frac{2\pi}{\lambda}*\cos\theta_1*h) = \text{sinc}^2(\varepsilon \frac{h}{\lambda}) = f(\frac{h}{\lambda})$$

where $\varepsilon = 4\pi\cos\theta_1 = $ constant

Keeping h constant and varying λ we see that for $\lambda_1 > \lambda_2$

$$Is_1 > Is_2$$

which shows light with larger wavelength sees a surface as a smooth one which on the other hand may be rough for light with smaller wavelength. For example the radio waves are simply reflected specularly by clouds, trees, houses etc. while the sunlight is totally scattered or diffused.

2.5 ASSUMPTIONS

The assumption used while deriving (28) section 2.1 and (7) section 2.8 are :

(A) The surface is perfectly conducting and quantities a and b in (17), (18) section 2.1 are constant.

(B) Mutual interaction of irregularities (shadowing or multiple scattering) may be neglected

(C) The incident plane wave is linearly polarized

(D) The point of observation is sufficiently far removed from the surface to regard the scattered waves as plane waves.

(E) Field at any point on the surface is expressed as sum of the incident and reflected field where R is the reflection coefficient of the plane tangent at the considered point ((5), section 2.1)

Assumption (E) implies that the surface undulations should be smooth and there should be no sharp corners. Hence in the present case of a triangular profile the theory is not applicable to the points 0, A and B. Fig. 2.7

CHAPTER 3

EXPERIMENTAL SET-UP AND PROCEDURE

In the present work effort is done to relate the AD of scattered light to surface microtopography. To perform the experiment few things such as a laser, photo-detector, a rough surface, multimeter and a AD measuring instrument are necessary. Due to non-availability of any instrument for measuring AD a new one had to be designed and fabricated. Measurement of AD requires that the rough surface specimen be kept fixed' w.r.t laser while the detector rorates about the point of incidence on the rough-surface specimen. Since AD depends upon the angle of incidence also, a provision for change of angle of incidence is also necessary. To achieve the above two motions following requirements came forward and their solutions were found, which crystallised into the instrument shown in Fig.3.1.

Some of the salient features of the instrument are (Fig.3.1):

a. Three rotational and one translational motion along Z-axis for the detector

b. One translational motion along Y-axis for the whole system

c. Two translational motion along Z and Y-axis and one rotational motion about Z-axis for the specimen

d. Minimum rotational motion possible for the detector with hand is 0.1 degrees

e. An unconventional method of measuring AD, in which detector is kept fixed while the specimen rotates [11], is also possible with this system.
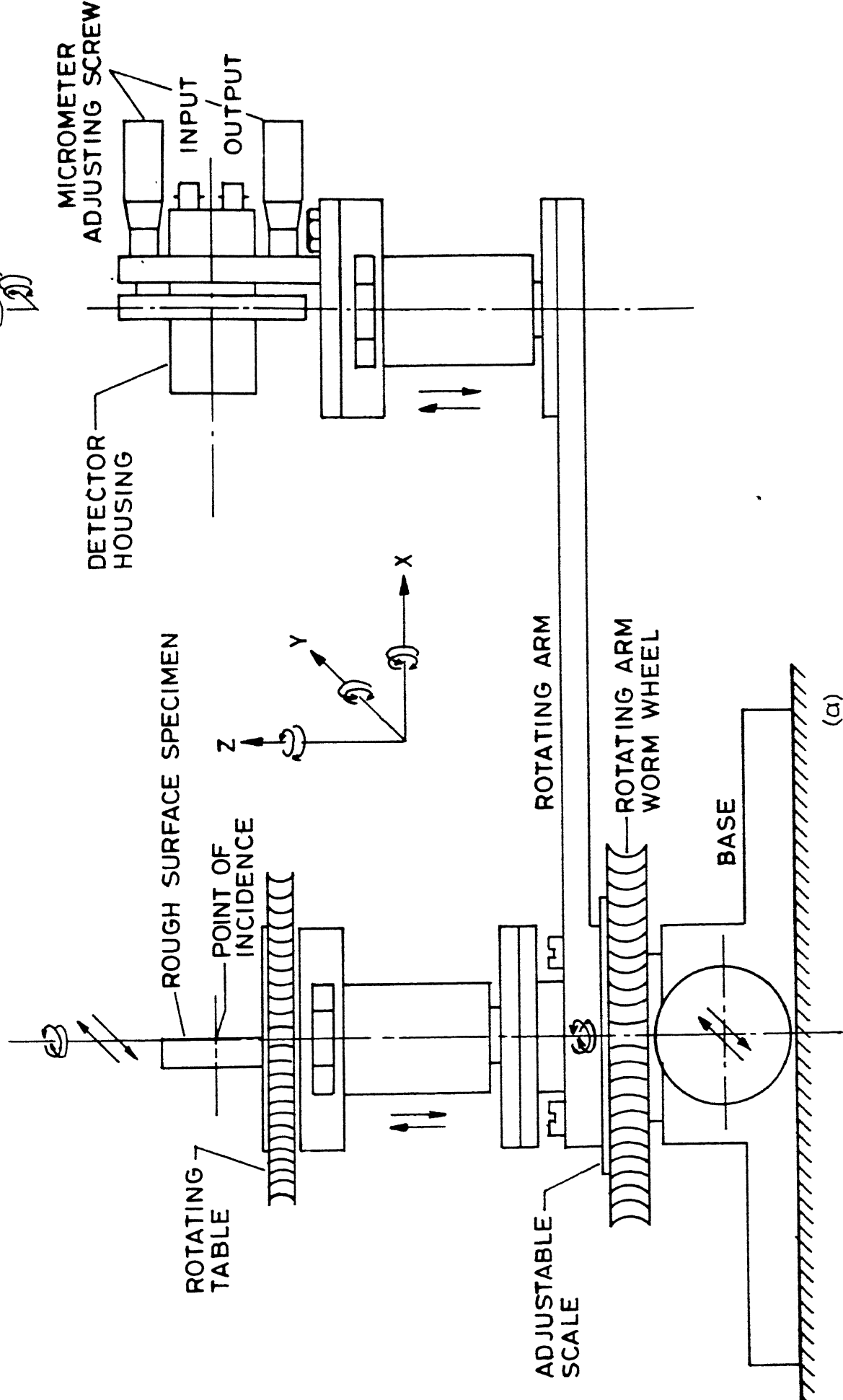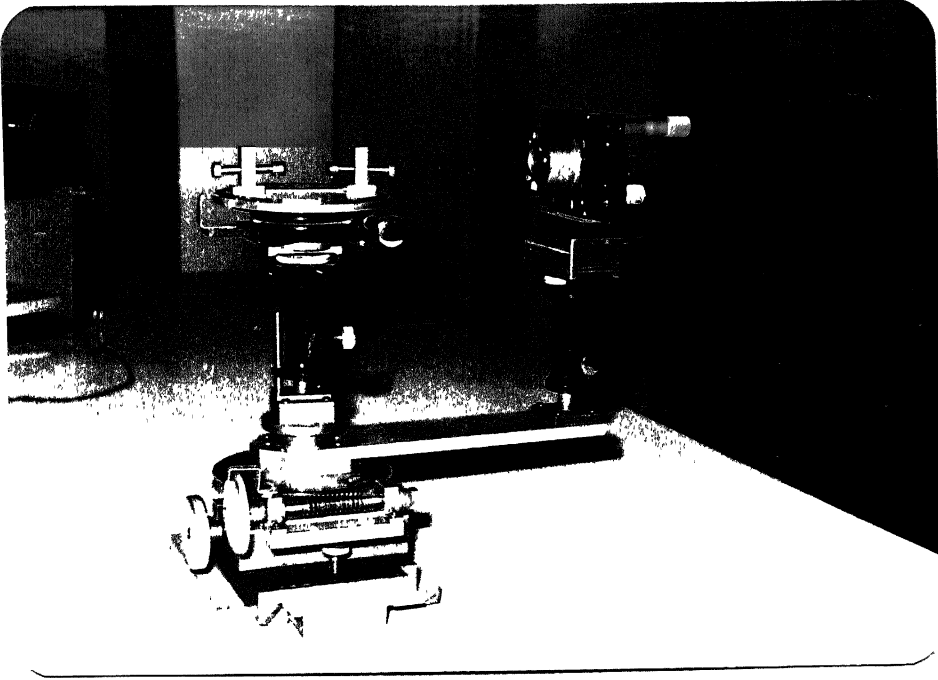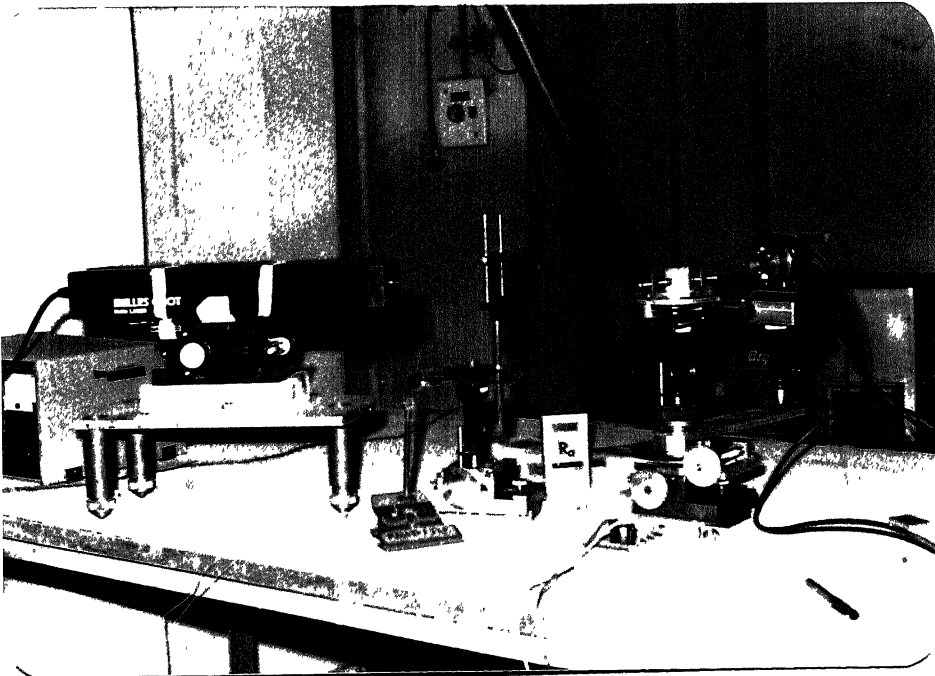
43

FIG. 3.1 SCATTERED INTENSITY MEASURING INSTRUMENT.

(b)

(c)

FIG. 3.1 (CONTD.)

3.1   EXPERIMENTAL SET-UP

Following steps are taken before setting up the experiment:

3.1.1   *Selection of laser*: Scattering of light from a rough surface depends upon the angle of incidence and wavelength of light source. Furthermore light is scattered in all directions, hence an intense source of light is desirable so that light scattered in a particular direction is of measurable amount. Laser is a source of highly monochromatic and intense beam of light. Combined with its directionality, it is the ideal light source for the experiment.   A 5mW `Melles-Griot' He-Ne laser polarised in the plane of incidence, $\lambda = 6328.193$ A$^{\circ}$, is used in the experiment (Fig.3.1-c). Since He-Ne lasers are commercially available and their wavelength lies in the visible range, hence their applicability in the present work.

3.1.2   *Selection   of   photo-detector*:   C30808   P-i-N phototransistor (Fig.3.4) sensitive to He-Ne laser wavelength with the specifications given in Table 3.1 is used for experimentation. Responsivity of detector is calibrated experimentally (Fig.3.2). The detector housing is designed (Fig.3.5) incorporating an amplifier circuit (Fig.3.3). Care is taken that the detector output does not exceed the saturation voltage of 47.3V while performing an experiment. Assuming that intensity falling on the detector is constant over its entire sensitive area for any scattering direction θ_s w.r.t. θ_i the output of detector is proportional to the intensity of scattered light. The solid angle substended by detector on the rough surface needs to be small so as to allow minimum diffused light and large enough so as to receive all the light scattered in a particular direction

Table 3.1

PHOTODIODE SPECIFICATIONS

e	Photosensitive surface		Typical spectral response range 10% point	Maximum Ratings					Field of view (degree)
				D.C. Reverse voltatge V_{pm}	Photocurrent density I_P		Forward current I_F		
	Area	Dia			Av. DC Valve	Peak Valve	Av. DC Valve	Peak Valve	
	mm^2	mm	nm	V	mA/mm^2	mA/mm^2	mA	mA	
C 308	5	2.5	400 to 1100	100	5	20	10	100	72
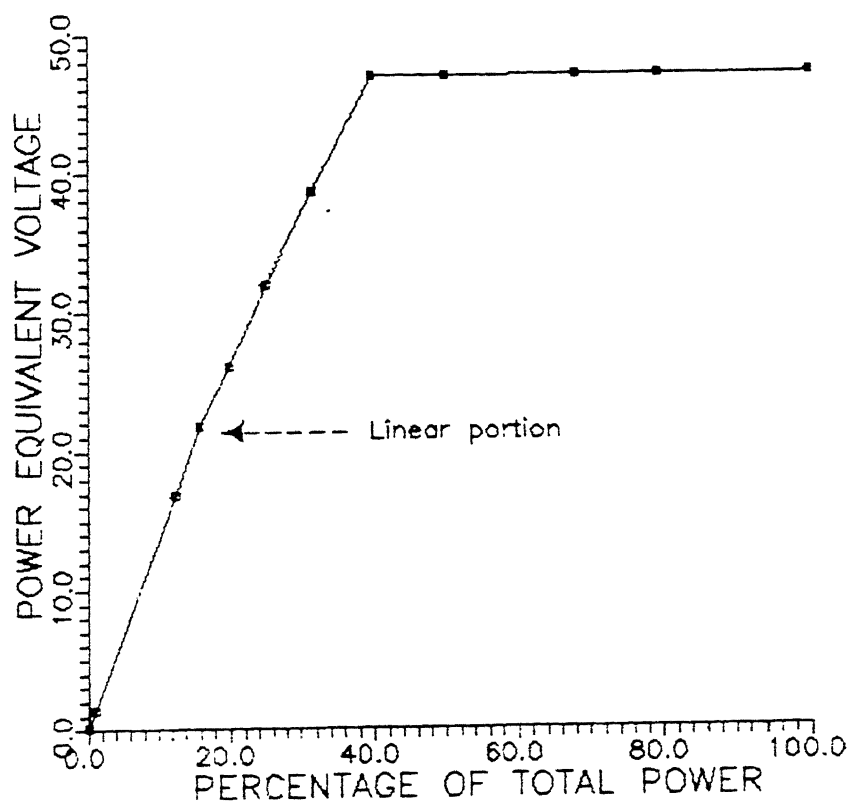
FIG 3.2   PHOTODIODE RESPONSIVITY CURVE
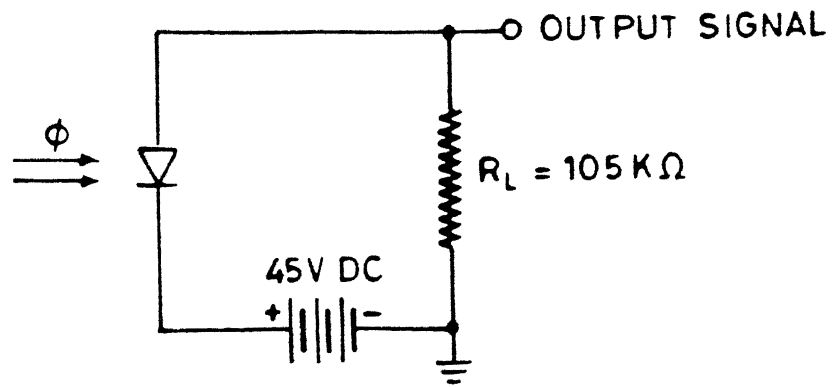
FIG. 3.3 AMPLIFIER CIRCUIT
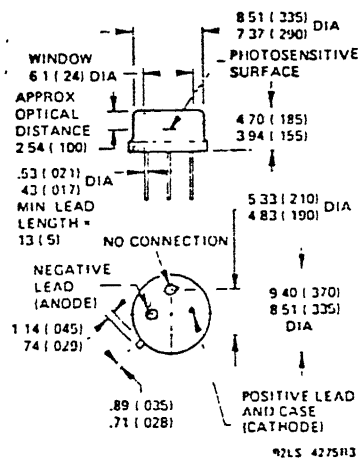
Dimensions in millimeters. Dimensions in parentheses are in inches

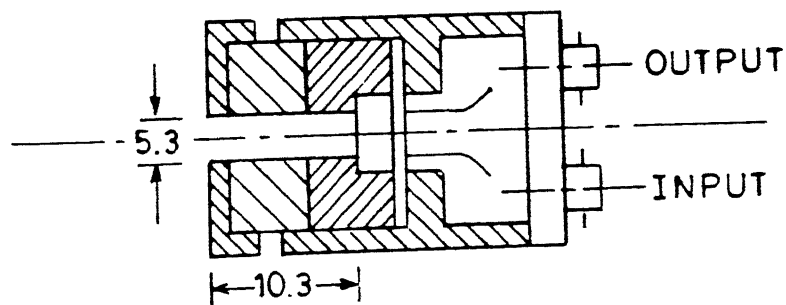## FIG. 3.4 C 30808 PHOTOTRANSISTOR.

FIG. 3.5 X-SECTION OF DETECTOR HOUSING.

(Fig.3.6).

P' = Point of incidence on specimen

DD' = detector sensitive area = 2.5mm dia

RR = distance of detector from specimen = 230mm

solid angle substended $\theta = \dfrac{\Pi(DD')}{2(RR')^2} = \dfrac{\Pi(2.5)^2}{4*52900} = 0.0001$ steridians

Total surface VV' viewed by detector (Fig.3.7)

$= \dfrac{2rR}{x} = \dfrac{5.3 \times 230}{10.34} = 117.8$ mm $>$ laser spot size on the surface

3.1.3 *Detector motion:* Intensity is the rate of flow of energy per unit area and in case of scattering the intensity in a particular direction goes on decreasing with distance, because the scattered light expands in space. Hence the detector is required to move in a radius about the point of incidence, so as to measure intensity at the same distance from the point of incidence. Hence detector is mounted at the end of a rotating arm whose axis of rotation coincides with the axis of rotation of rotating table on which rough surface specimen is mounted.

3.1.4 *Point of incidence:* Angular distribution of scattered light can change with the point of incidence on the rough surface specimen. Hence the point of incidence on the rough surface specimen should coincide with the centre of rotation of rotating table on which the specimen is placed (Fig.3.1). Else the point of incidence changes as the incidence angle is changed. This is
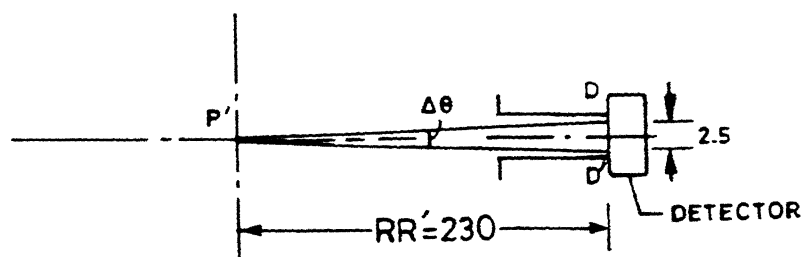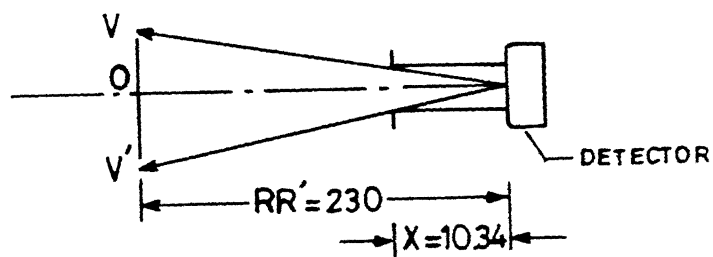
FIG. 3.6 SOLID ANGLE SUBSTENDED BY DETECTOR.

FIG. 3.7 SURFACE VIEWED BY DETECTOR.

also shown geometrically for two possible cases, namely, when point of incidence does not coincide with centre of rotation of specimen, centre of rotation of specimen coincides with centre of rotation of rotating table (Fig.3.8-b). Then point of incidence changes by

$$\delta = AC-AB = x \; \frac{\cos(\theta_i - \alpha) - \cos\theta_i}{\cos(\theta_i - \alpha)}$$

and secondly, when, centre of rotation of specimen does not coincide with centre of rotation of rotating table (Fig 3.8-c)

$$Change = AB = r \; \frac{\tan\alpha.\cos(\alpha - \theta_i) - (\sec\alpha - 1)\sin\theta_i}{\cos(\alpha - \theta_i)}$$

r = radius eccentricity

θ_i = angle of incidence

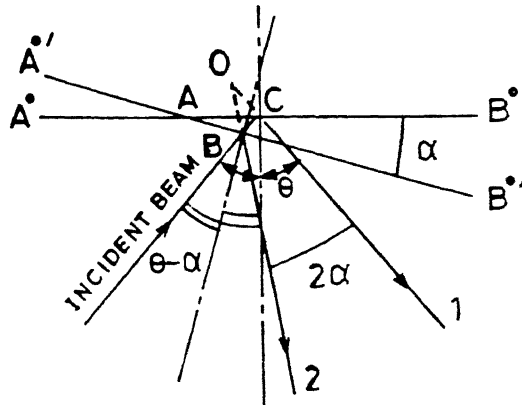α = change in angle of incidence

The motion of both specimen and detector is achieved by worm and worm wheel arrangement designed by Lewis equation and are fabricated outside Kanpur.

3.1.5   *Need for vertical motion* (Fig.3.1): It is observed that for highly periodic surface the light is scattered perpendicular to the direction of *lay at the point of incidence. Since the detector rotates in horizontal plane only. Hence need of vertical motion along Z-axis for the specimen is required so as to make scattered pattern horizontal (Fig.3.12-a) by changing the point of incidence. Also a horizontal motion along Y-axis is incorporated so as to make scanning of whole rough surface possible by combination of motion along Y and Z-axis. Detector vertical motion is also desired so that the detector properly accepts the scattered intensity pattern.
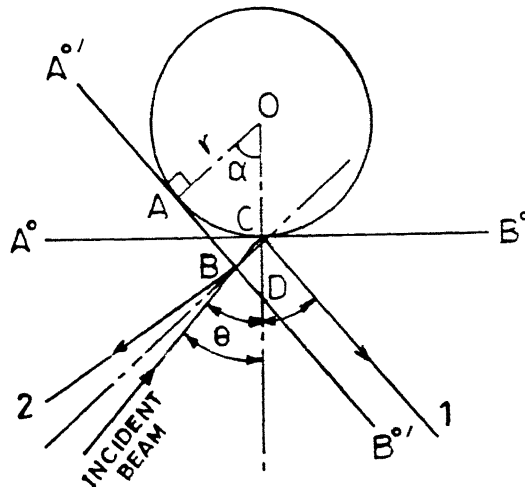
---

* In the present work the lay of the rough surface specimens (rss) has a circular curvature.
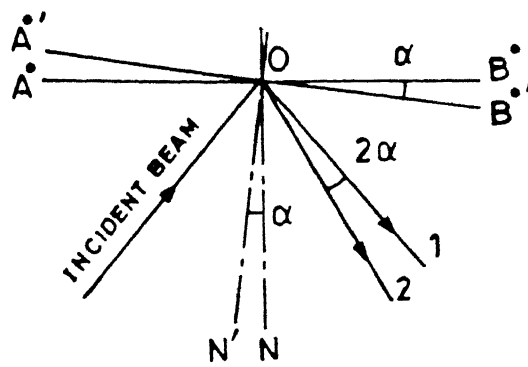
(a) POINT OF INCIDENCE = POINT OF ROTATION
A⁰B⁰ = SPECIMEN SURFACE

(b) POINT OF INCIDENCE ≠ POINT OF ROTATION

(c) POINT OF ROTATION NOT ON SPECIMEN SURFACE

FIG. 3.8 EFFECT ON POSITION OF POINT OF INCIDENCE WITH CHANGE IN ANGLE OF INCIDENCE BY ROTATING THE SPECIMEN.

scattered intensity pattern.

3.1.6 *Mirror mounts*: The detector should be perpendicular to the surface of the specimen at the point of incidence. Hence the detector housing is mounted on mirror mount and initial adjustment is done by replacing the specimen by mirror mounted on mirror mount. Such that the the front surface of mirror coincides with axis of rotation of rotating table (Fig.3.9-a). First of all the mirror is made perpendicular to the laser with the help of micrometer adjusting screws. Then the rotating table is rotated by an angle θ_1 equal to the angle of incidence. Then the detector is brought in the path of the laser beam reflected from the mirror surface, such that the beam hit the detector sensitive area through the apprture. The detector now is fixed in specular direction. Then a mirror is plugged into the detector aperture and the detector is adjusted till the reflected ray retraces its path (Fig.3.9-b) the rotating arm scale is then adjusted to zero and mirror is taken out of the detector aperture. And the mirror placed on the rotating table is replaced by a rough surface specimen.

3.1.7 *Shape of rough surface specimens(rss)*: Rectangular aluminium test specimens of 30mm 30mm × 10mm are made and one of their flat surface is machined giving 30mm × 30mm of rough surface. Specimen are made on both milling and lathe machine with different cutting conditions so as to have surfaces with different roughness. On the whole fifteen specimens are made to the specifications given in table 3.2. Due to the shape of the tools used both for milling

Table 3.2

SPECIFICATION OF SPECIMENS

(a) FACE TURNING

| imen	Feed mm/Rev	R.P.M	Depth of Cut (mm)	R_a (Measured value) microns(μ)
	1.596	421	0.2	15.6
?	0.638	421	0.2	3.8
?	0.199	646	0.2	1.0
	0.049	421	0.1	0.8

(b) FACE MILLING

:imen o.	Feed (mm/rev)	Cutting speed (m/min)	Depth of cut (mm)	R_a	Nose radius (mm)	* Effective tool angles (Deg.)	
						End Cutting Edge	Side Cutting Edge
.	0.01	504.5	0.2	1.5	0.25	18°	0°
?	0.02	504.5	0.1	1.4	0.25	18°	0°
?	0.06	319.6	0.1	1.5	0.25	18°	0°
4	0.043	504.5	0.2	1.6	0.25	18°	0°
5	0.045	190	0.2	0.9	1.25	22°	21.25°
6	0.017	504.5	0.2	0.3	1.25	22°	21.25°
7	0.007	781.7	0.2	0.3	1.25	22°	21.25°
8	0.011	781.7	0.15	0.4	1.25	22°	21.25°
9	0.017	319.65	0.1	0.7	1.25	2°	34°
10	0.01	504.5	0.2	0.4	1.25	2°	34°
11	0.007	781.7	0.1	0.3	1.25	2°	34°

* Flytool is inclined at 39° with the vertical.
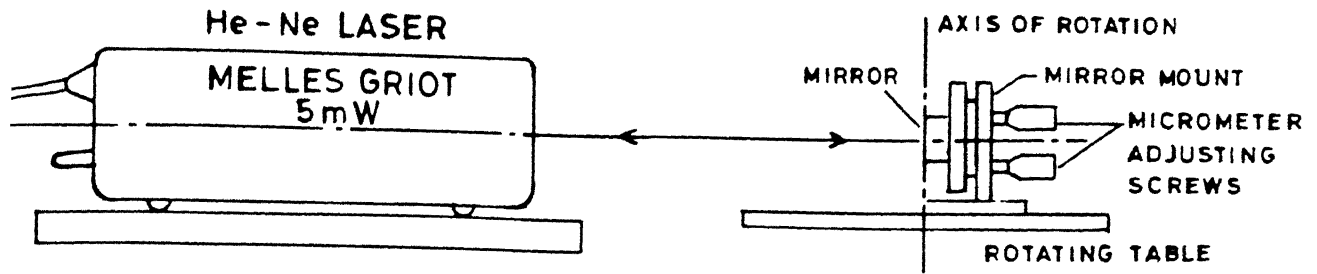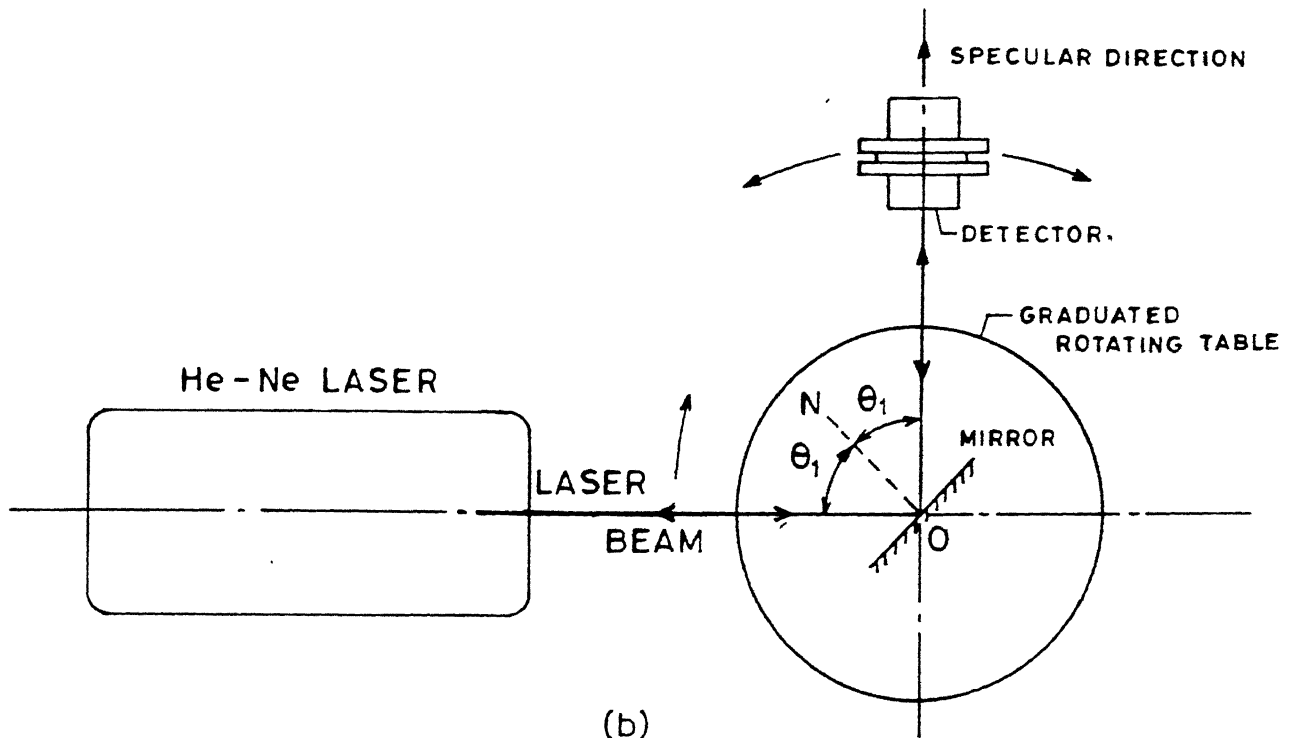
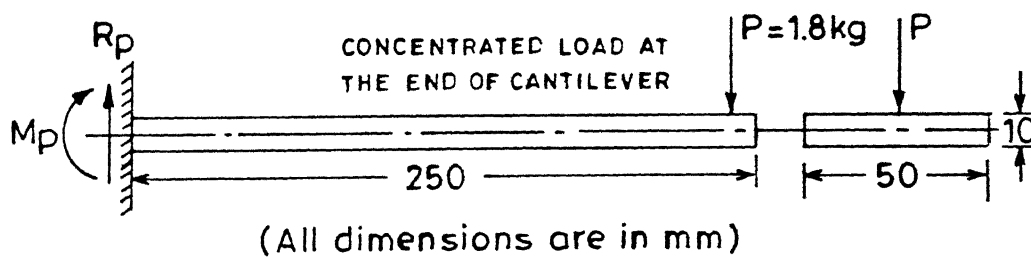## FIG. 3.9 ALLIGNMENT OF DETECTOR AND LASER.

FIG. 3.10 DETECTOR ARM.

and facing (Fig.4.9-a), it is justified to assume that the undulations on the surface are triangular. Figure 4.8 shows the actual profile measured by Talysurf-10 roughness measuring instrument for some of the specimens.

3.1.8   *Distance of the detector from the specimen*: A compromise between the two requirements, that is, one; the point of observation should be in Fraunhofer zone and, second; that the detector should move in a radius about the point of incidence, needs to be made. Since the detector is mounted at the end of rotating arm which can be assumed as an cantilever having concentrated load at the end (Fig.3.10). Hence there is a limitation to the length of the detector arm. The calculated maximum length in our present case comes out to be 250mm.

3.2   PROCEDURE

Figure 3.1-c and Fig.3.11 shows the schematic diagram of the experimental set-up. The prepared aluminium specimens are procured from the workshop and preserved in polythene bags. The laser is inclined at 25° to the Y-axis and is at a distance of 350mm from the rough surface specimen. The spot size on the specimen is about 1.8mm in diameter. Before start of the experiment, lights are switched off and the experiment is performed in dark.

3.2.1   *Angular distribution (AD) measurement*: After the initial adjustment as explained in article 3.1.6, the specimen is moved till the diffraction pattern is horizontal (Fig.3.12-a) and passes

through the detector aperture. Readings are then taken at a $1/2^O$ interval both in clockwise and anticlockwise direction about the specular beam. Measured values are marked +ve which are taken away from the laser or in clockwise direction about the specular beam for the present configuration and -ve for those readings taken in anticlockwise direction, i.e. towards the laser as shown in figure 3.11. Then these measured values of voltage are plotted against $(\theta_s - \theta_i)$. Where θ_s is the scattering angle w.r.t normal. AD is measured at different angles of incidence (θ_i) and for different specimens.

3.2.2 *Measurement of specular intensity*: This involves changing the angle of incidence by rotating the specimen. The detector has to move twice the angle moved by specimen, to remain in specular direction. The initial adjustment is done by rotating the detector such that it directly faces the laser beam. Then the specimen is inserted in between and aligned at 90° to the laser beam. Readings are taken at 1^O interval and measured values of voltage are plotted against the angle of incidence.
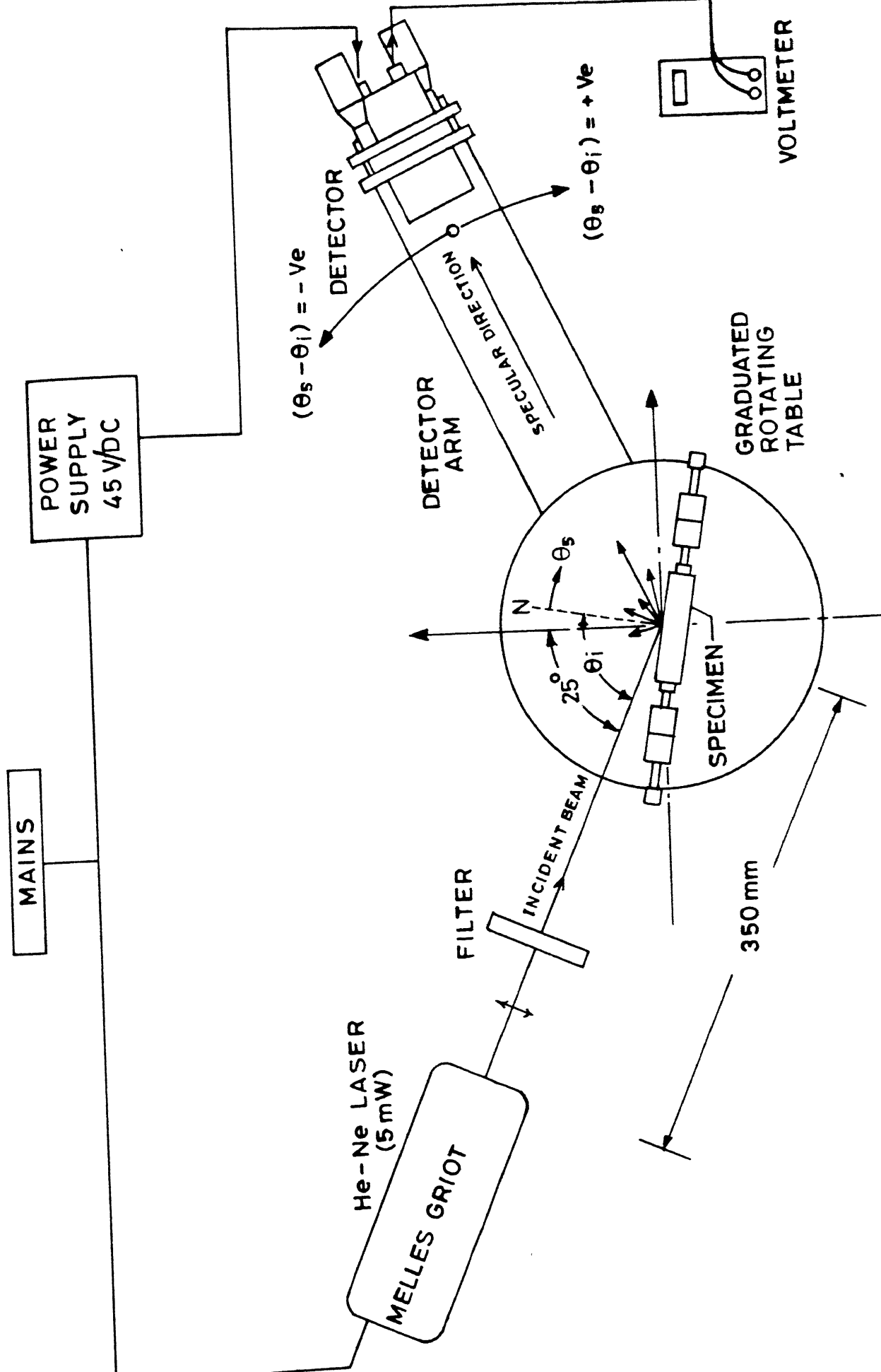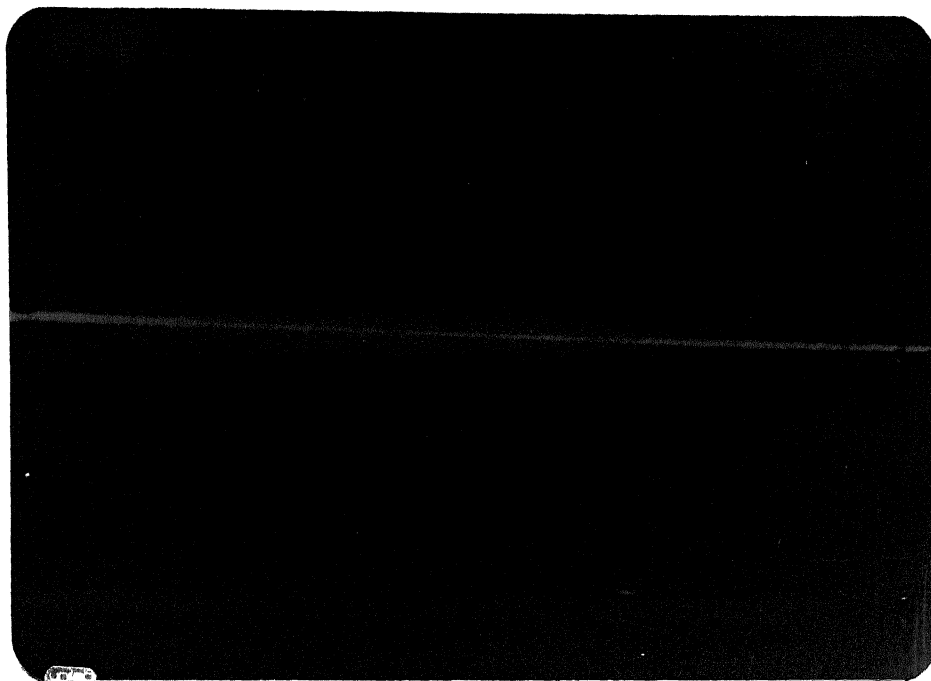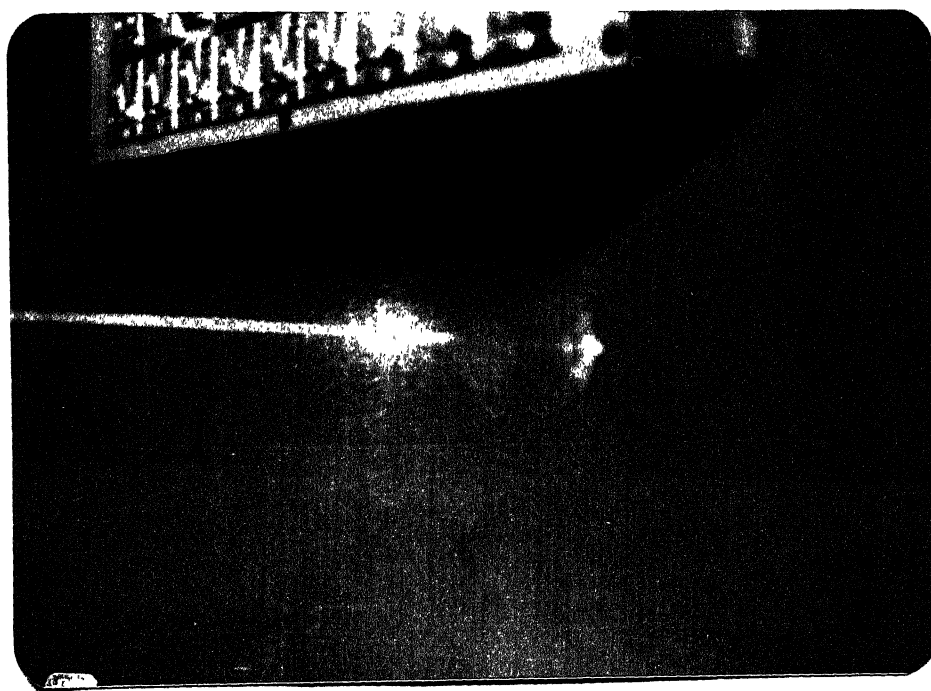
FIG.3.11 SCHEMATIC DIAGRAM OF EXPERIMENTAL SET UP.

(a) $\theta_i = 45°$

(b) $\theta_i = 87°$

FIG.3.12 DIFFRACTION PATTERN AT DIFFERENT
ANGLE OF INCIDENCE.

CHAPTER 4

EXPERIMENTAL RESULTS AND DISCUSSION

Angular distribution (AD) and specular intensity (I_s) is measured for incident angles of 0 to 90° by using He-Ne laser beam on specimens of aluminium machined by face turning and milling. The details of specimens and machining conditions are given in Table 3.2.

4.1 ANGULAR DISTRIBUTION

For AD measurement, the readings are taken at an interval of $1/2^O$ by rotating the detector while the specimen is kept fixed. Figures 4.1 to 4.4 are plots of AD obtained for face turned aluminium specimens FA-1 to FA-4 at various angles of incidence ranging from 0 to 75°. Figures 4.5 and 4.6 are plots of AD obtained for face milled aluminium specimens. MA-5 and MA-6 at various angles of incidence ranging from 0 to 87°. Table 2.1 gives the expected theoretical spacing between the modes for various specimens and calculated average spacing between the peaks (modes) for various plots, is also given in Table 2.1

4.2 SPECULAR INTENSITY

For specular intensity (I_s), the readings are taken by changing the angle of incidence by rotating the specimen at an interval of one degree as explained in article 3.2.2. Figures 4.7-a to 4.7-f are the plots of experimental and theoretical variation of I_s w.r.t angle of incidence for face milled specimens MA-5 to MA-10. The variation of angle of incidence is from 0 to 90°.
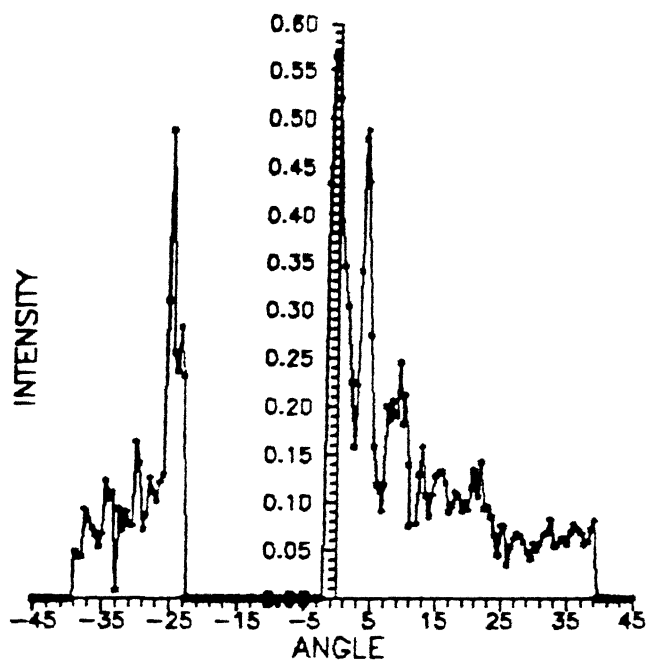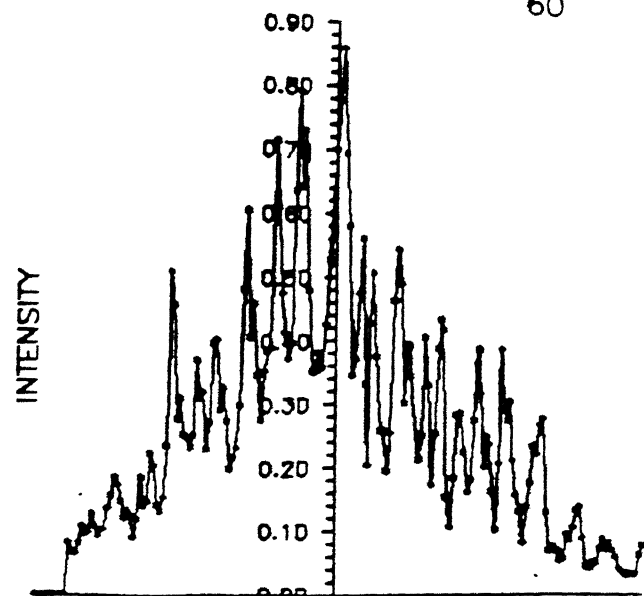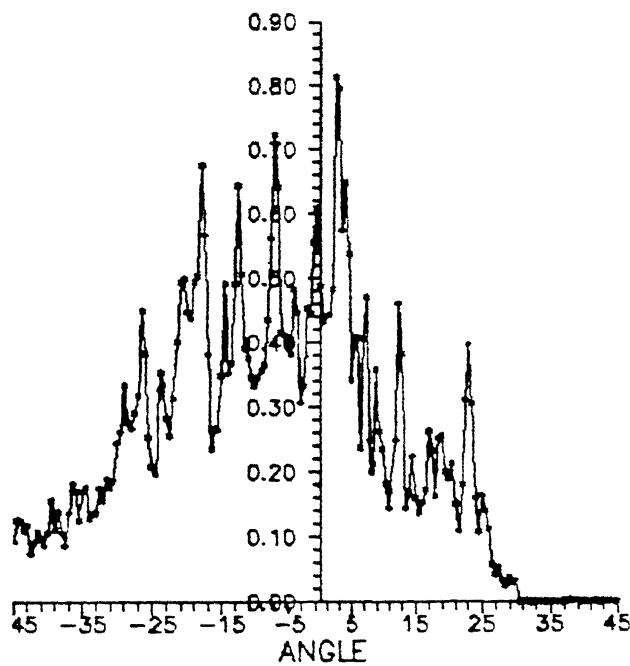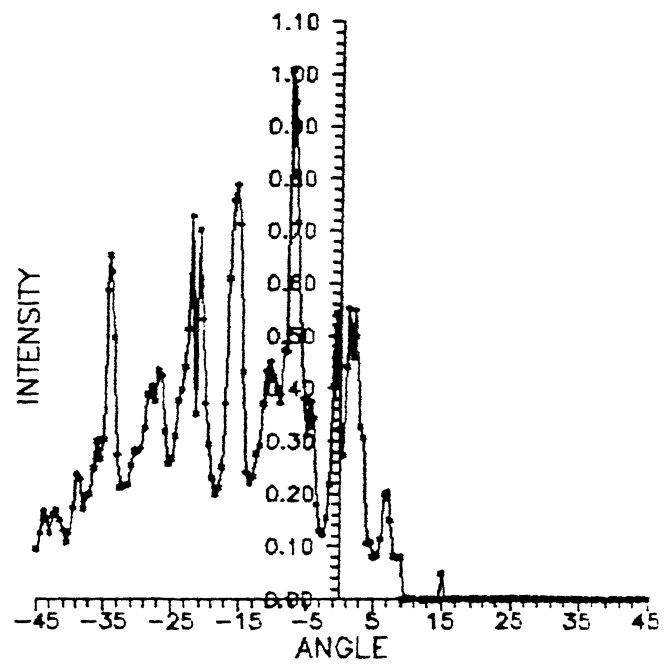
(a) $\theta_i = 5°$

(b) $\theta_i = 25°$

(c) $\theta_i = 50°$

(d) $\theta_i = 75°$

FIG. 4.1   AD MEASUREMENT FOR VARIOUS ANGLES
OF INCIDENCE FOR SPECIMEN NO. FA−1

(a) $\theta_i = 5°$

(b) $\theta_i = 25°$

(c) $\theta_i = 50°$

(d) $\theta_i = 75°$

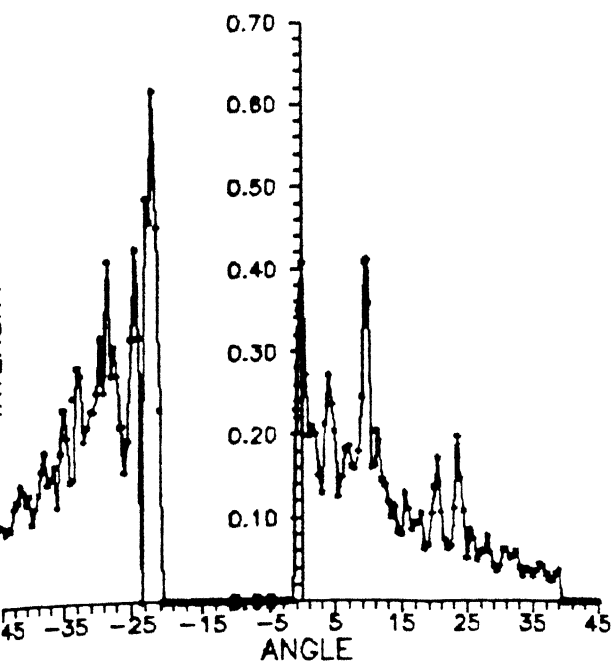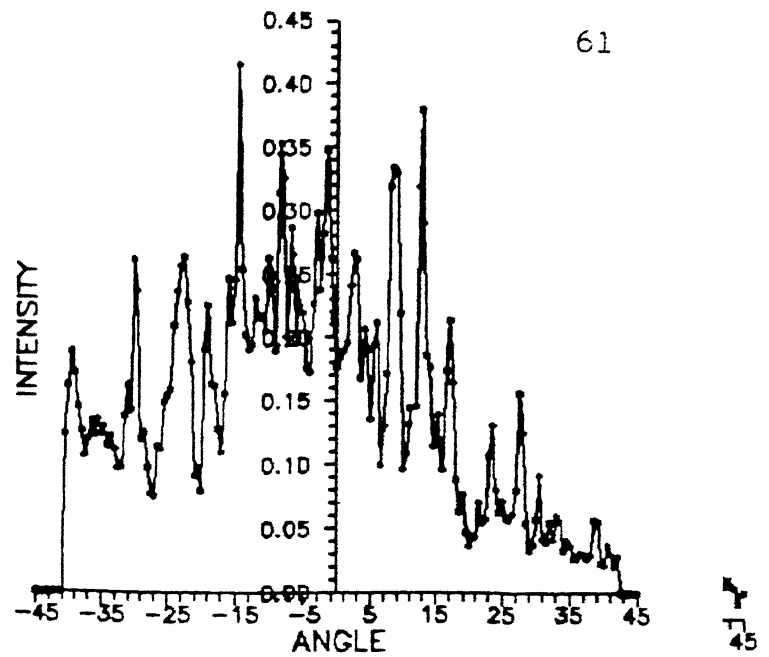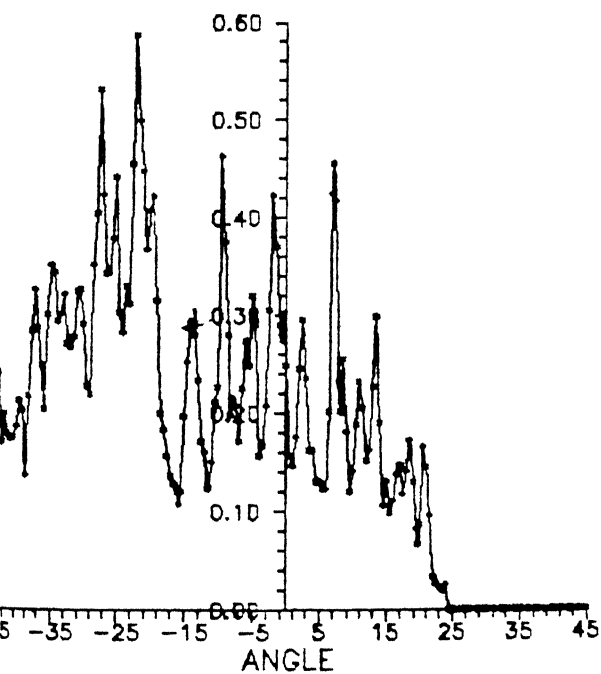FIG. 4.2   AD MEASUREMENT FOR VARIOUS ANGLES OF INCIDENCE FOR SPECIMEN NO. FA-2

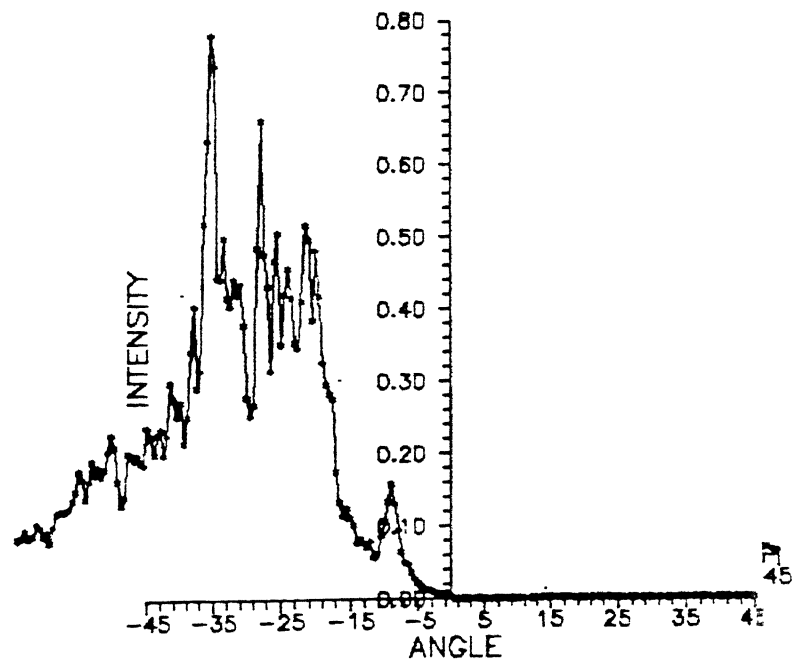(a) $\theta_i = 0°$

(b) $\theta_i = 5°$

(c) $\theta_i = 30°$

(d) $\theta_i = 40°$

FIG. 4.3   AD MEASUREMENT FOR VARIOUS ANGLES
OF INCIDENCE FOR SPECIMEN NO. FA-3
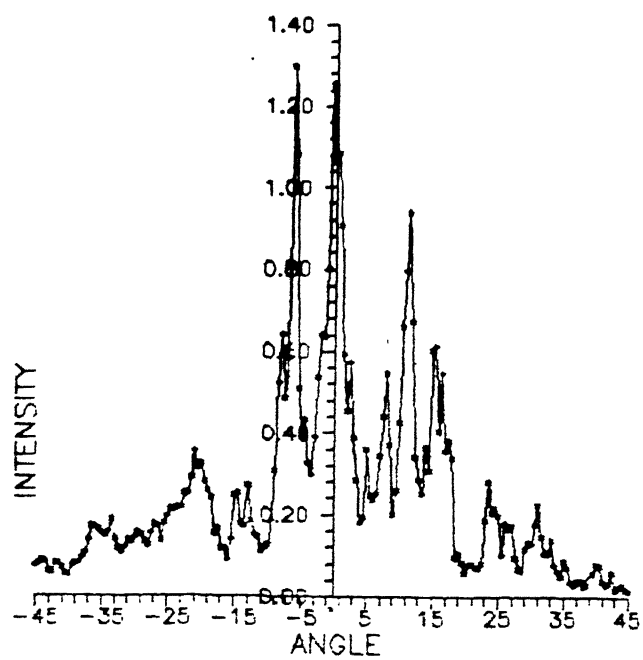
(e) $\theta_i = 45°$
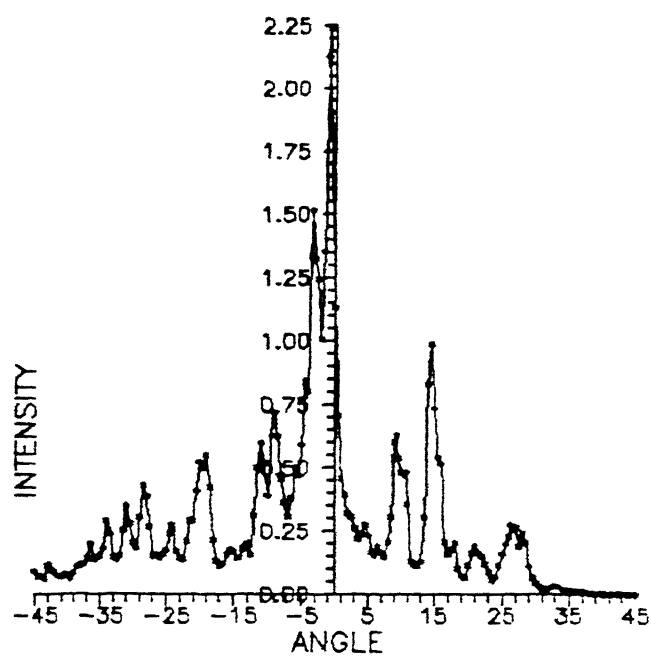
(f) $\theta_i = 55°$
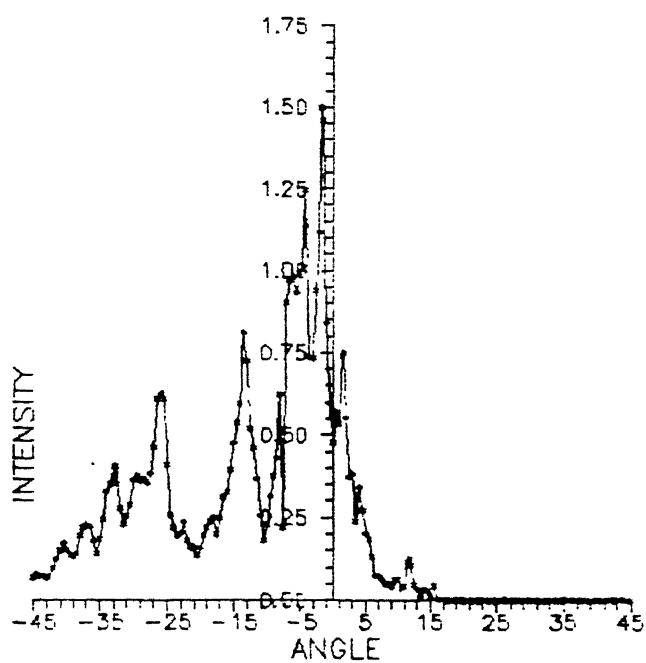
(g) $\theta_i = 75°$

FIG. 4.3 (contd.)
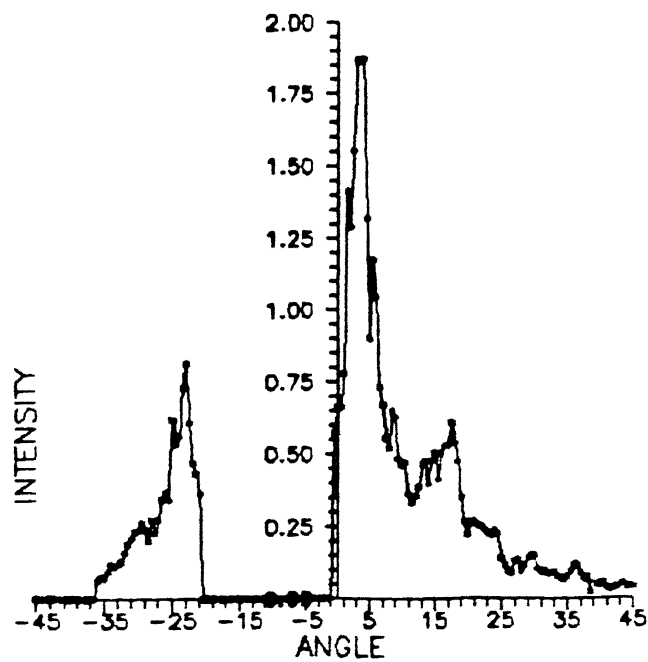
(a) $\theta_i = 5°$
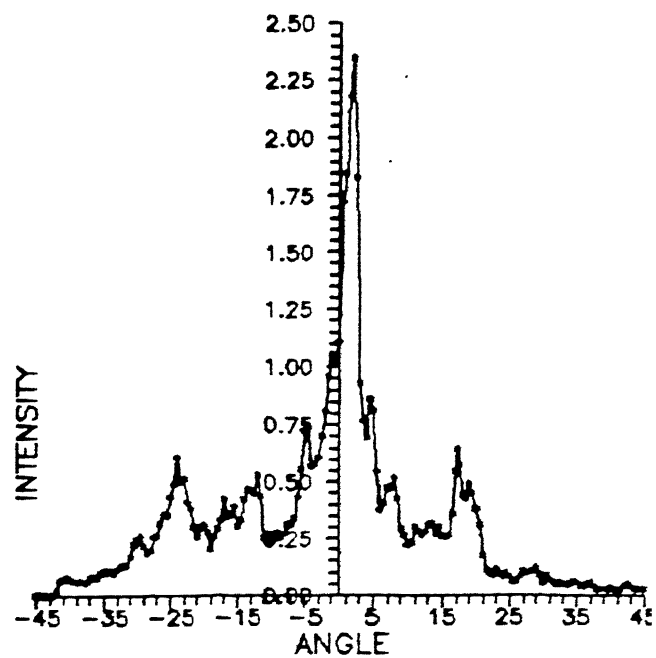
(b) $\theta_i = 35°$
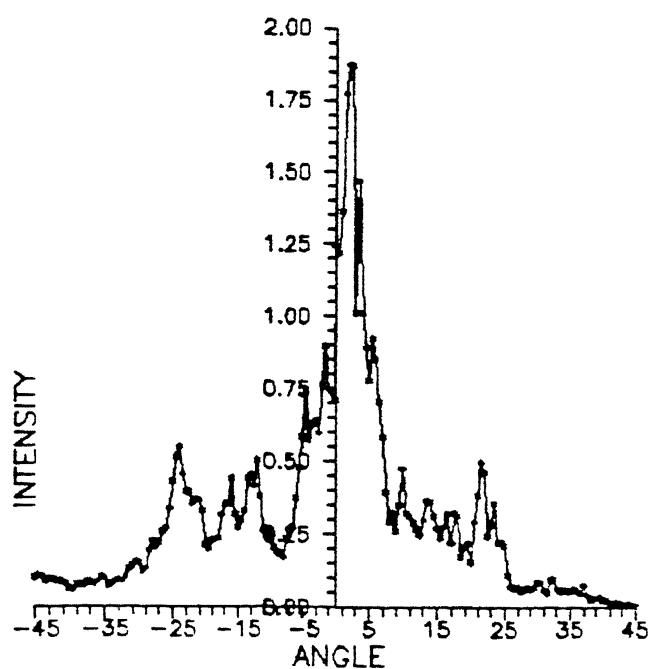
(c) $\theta_i = 45°$
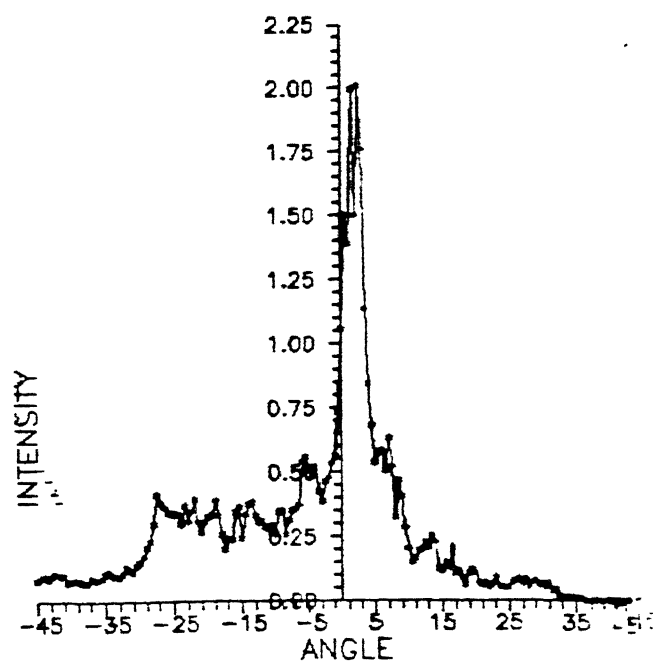
(d) $\theta_i = 50°$

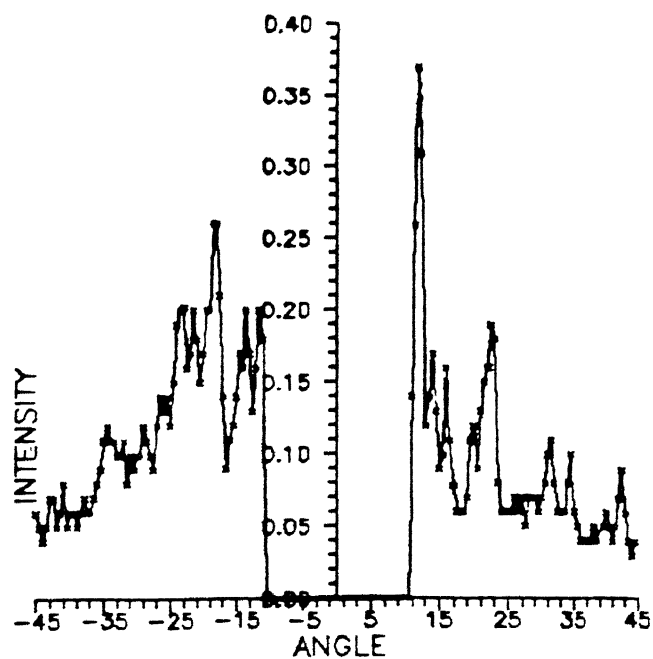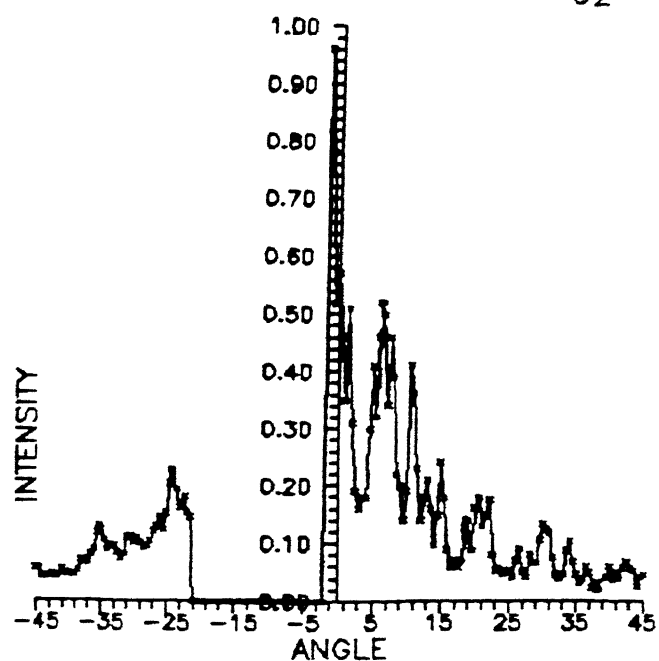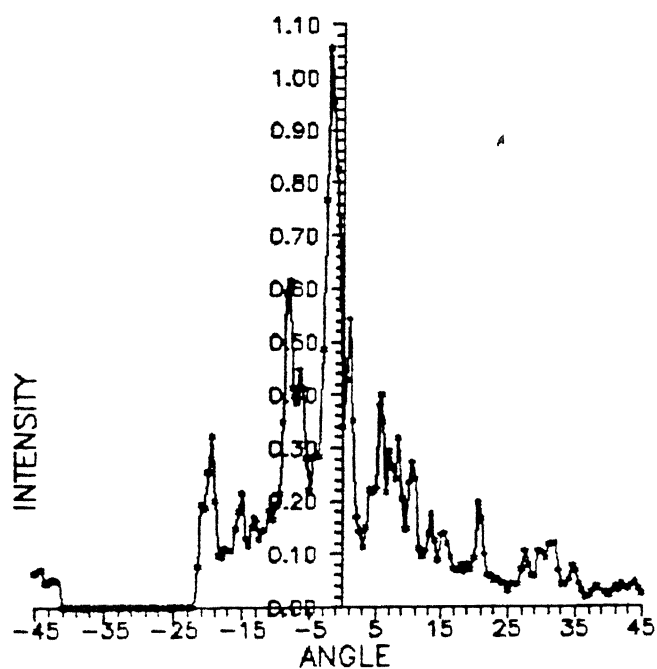FIG. 4.4   AD MEASUREMENT FOR VARIOUS ANGLES
OF INCIDENCE FOR SPECIMEN NO. FA—4
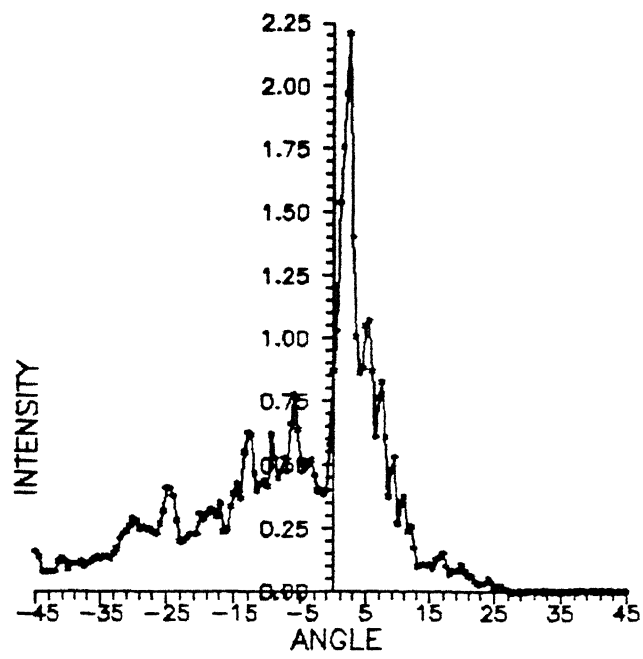
(e) $\theta_i = 60°$
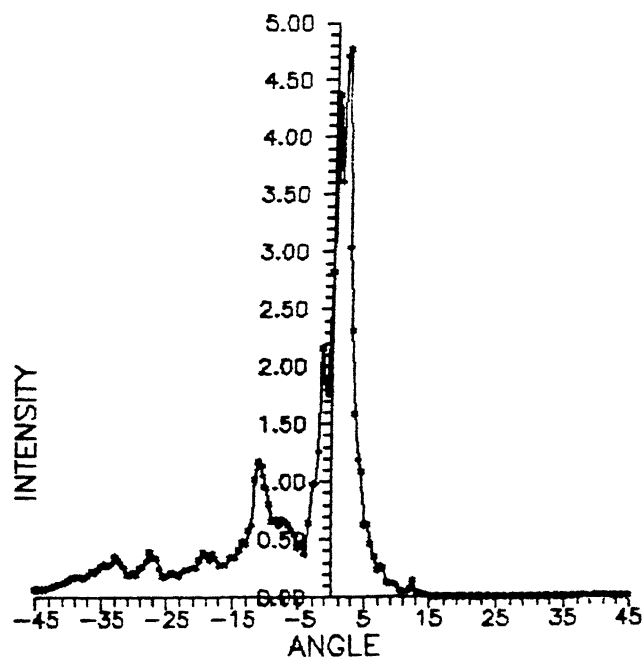
(f) $\theta_i = 75°$

FIG. 4.4 (contd.)
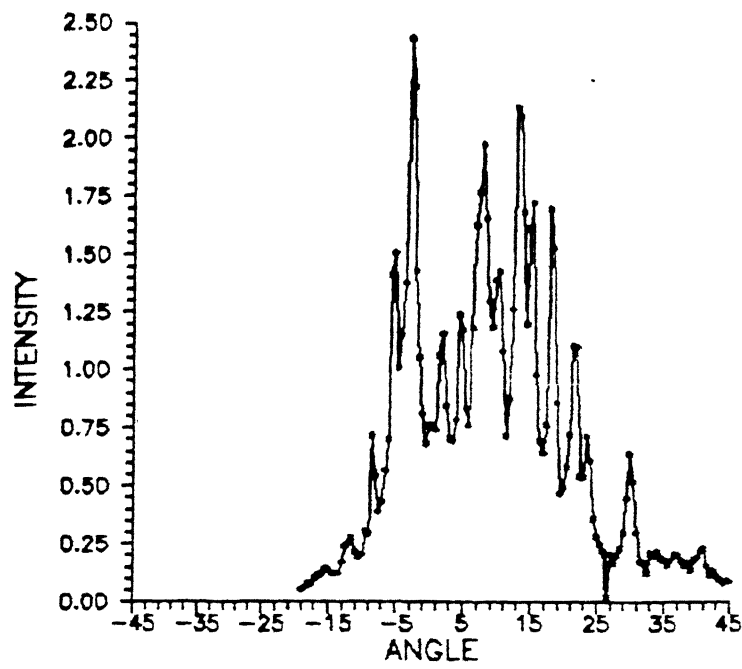
(a) $\theta_i = 10°$
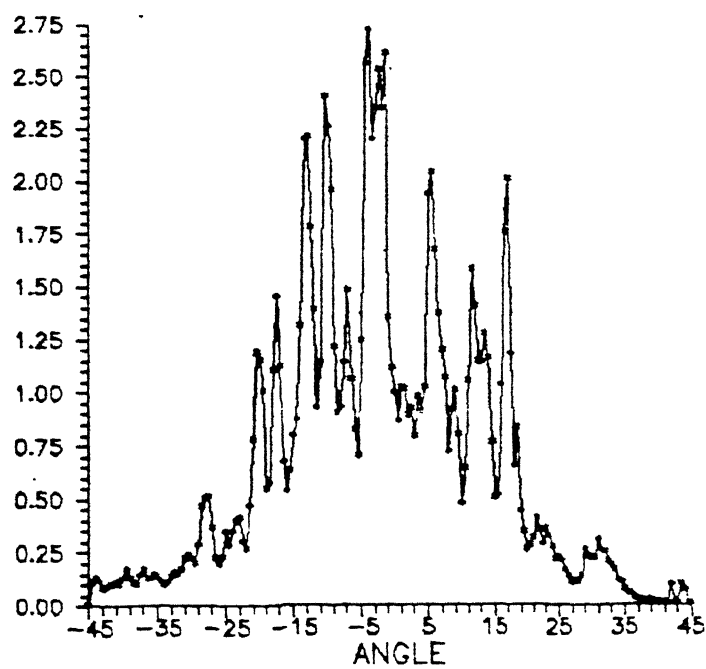
(b) $\theta_i = 45°$
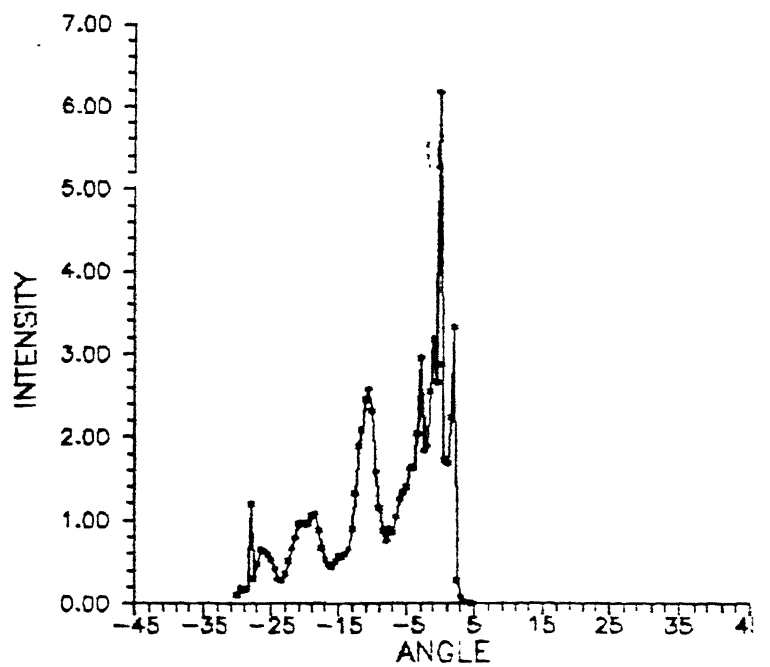
(c) $\theta_i = 86°$

FIG. 4.5   AD MEASUREMENT FOR VARIOUS ANGLES OF INCIDENCE FOR SPECIMEN NO. MA−5

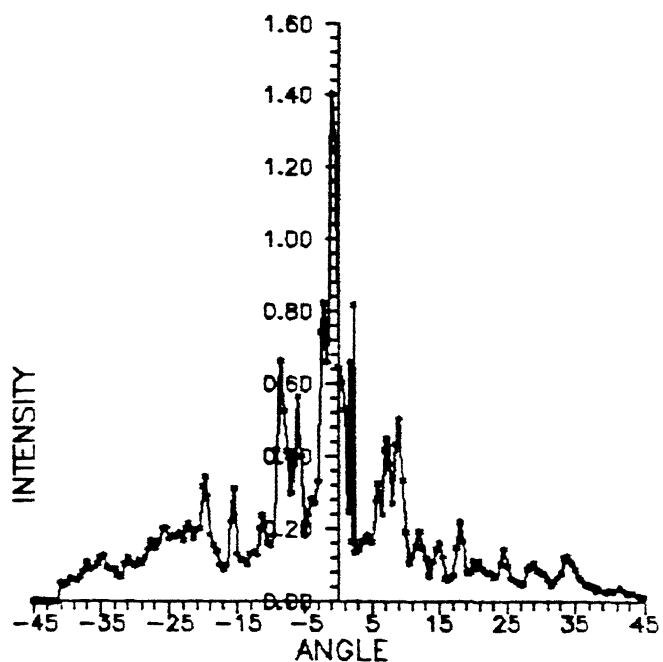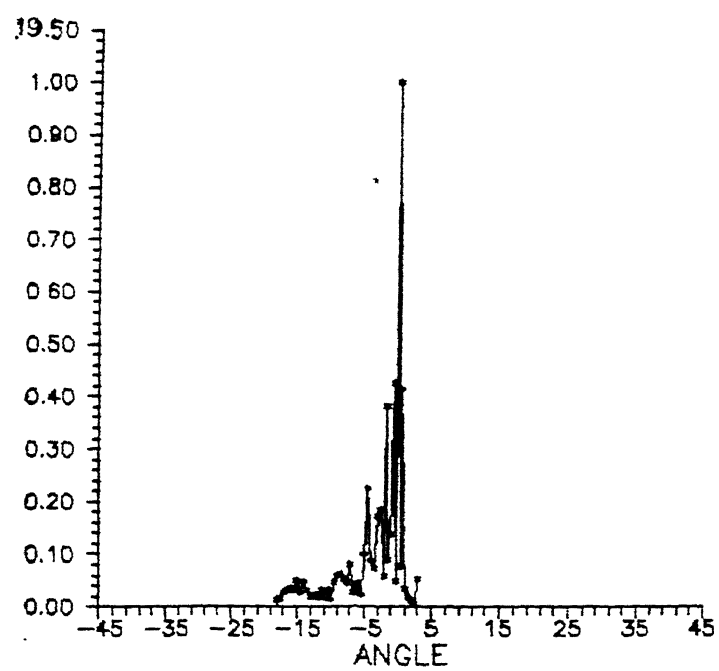FIG. 4.6 AD MEASUREMENT FOR SPECIMEN NO. MA-6
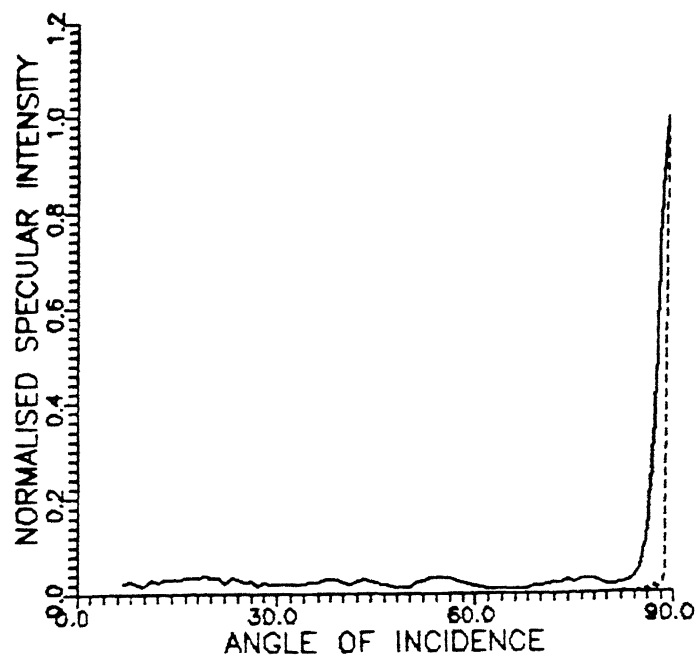
(a) SPECIMEN NO. MA − 5 : Ra − 0.9
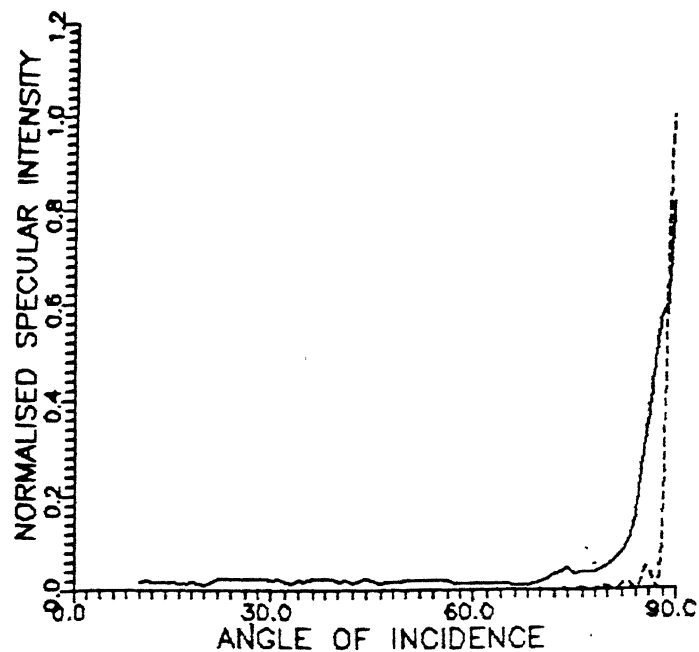
(b) SPECIMEN NO. MA − 6 : Ra − 0.3

——— EXPERIMENTAL

————— THEORETICAL
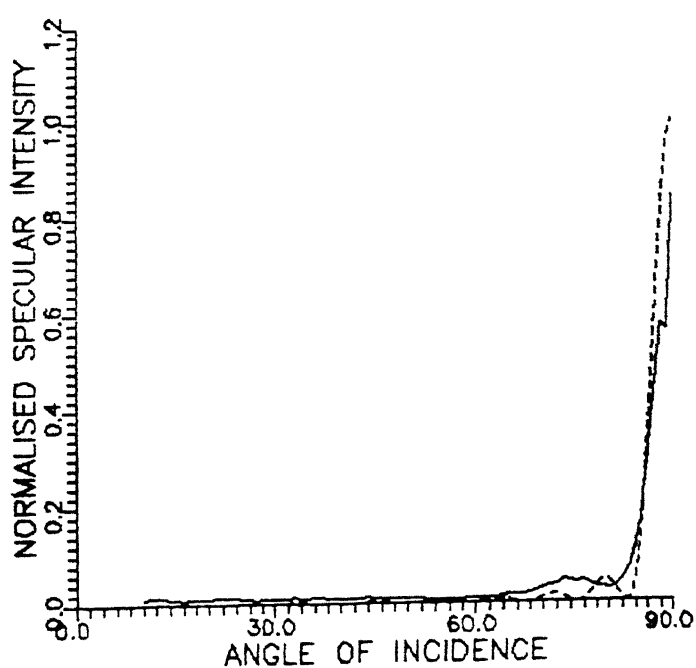
(c) SPECIMEN NO. MA − 7 : Ra − 0.3
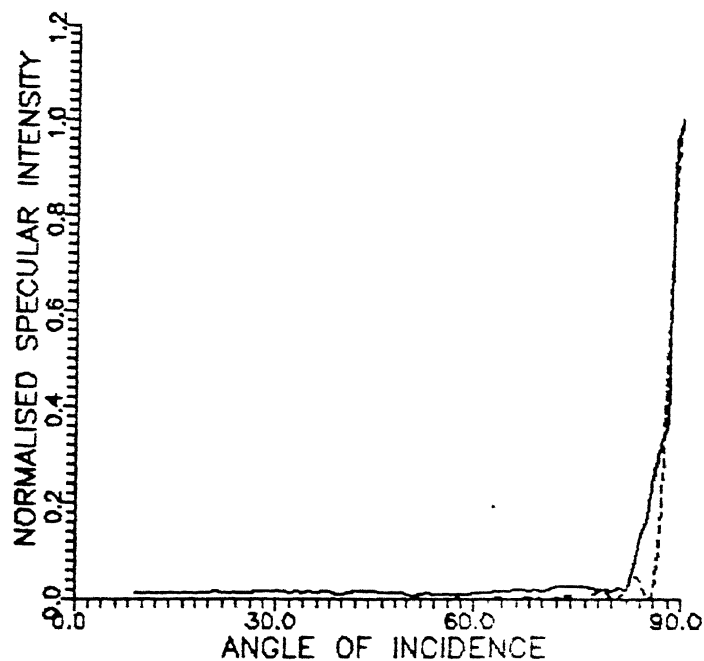
(d) SPECIMEN NO. MA − 8 : Ra − 0.4

FIG. 4.7 VARIATION OF SPECULAR INTENSITY WITH INCIDENCE ANGLE.

(e) SPECIMEN NO. MA — 9 : Ra = 0.7

(f) SPECIMEN NO. MA — 10 : Ra = 0.4
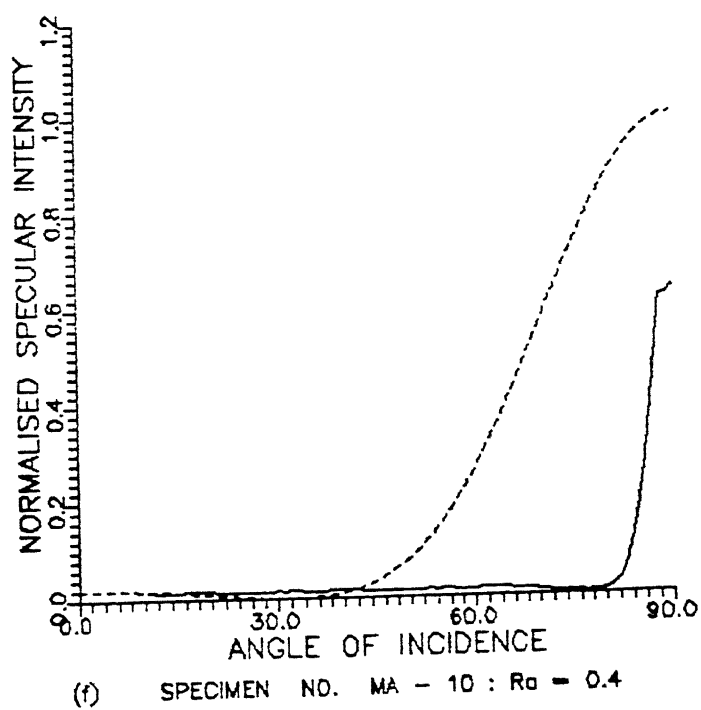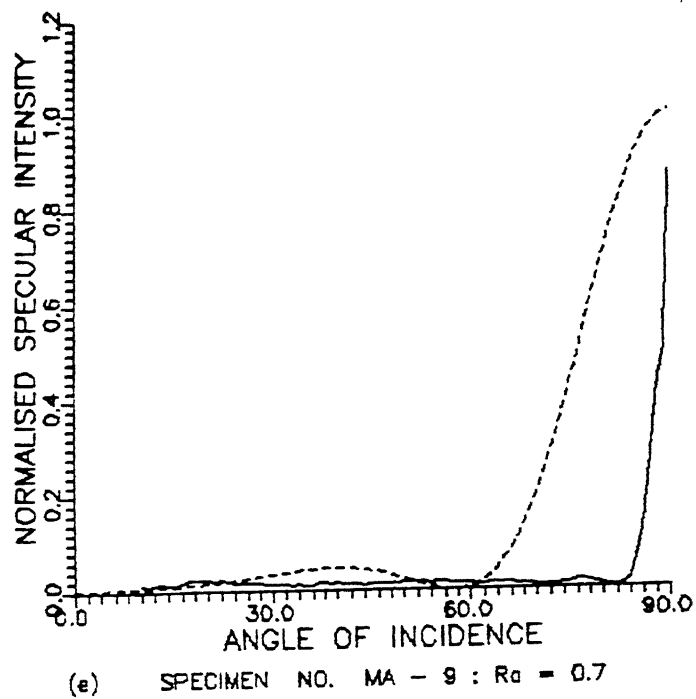
FIG. 4.7 (contd.)

4.3 ROUGHNESS PROFILE

Roughness records are taken by 'Talysurf-10 Roughness Measuring Instrument'. These records are shown for specimens FA-2 and MA-2 in Figure 4.8.

4.4 DISCUSSION

4.4.1 *Angular distribution*: All the AD plots show a No. of peaks. The peaks for specimen FA-1 (with higher R_a = 15.6μ), are very prominent, specially for θ_i = 25° and 50° (Figure 4.1) as compared to the peaks for specimen FA-3 for lower R_a = 1.0μ (Figure 4.3) and specimen FA-4, R_a = 0.8μ (Figure 4.4). For milling specimen MA-5, R_a = 0.9μ, peaks are distinctly seen for lower value of angle of incidence. However peaks come closer to the specular direction for specimen MA-6, R_a = 0.3μ (Figure 4.6).

Theoretical separation of these peaks are given in Table 2.1. The average spacing of the experimental AD measurements for some of the specimens is also given. Experimental values are much higher than the theoretical spacing of peaks. This may be due to the fact that the surface profile (Figure 2.7) may not be atriangular surface with smooth reflecting surface as assumed in the theory. Furthermore due to the corner radius of the order of 0.25mm to 1.25mm, the surface profile is expected to be circular with micro-irregularities as shown in Figure 4.9, specially at low feeds and depth of cut used in the experiment. Therefore it is not possible to relate the peak spacing from AD plots to spatial wavelength and roughness of surface.

4.4.2 *Specular Intensity*: Plots of variation of specular intensity with angle of incidence for different specimens show that all surfaces tend to reflect most of the incident light
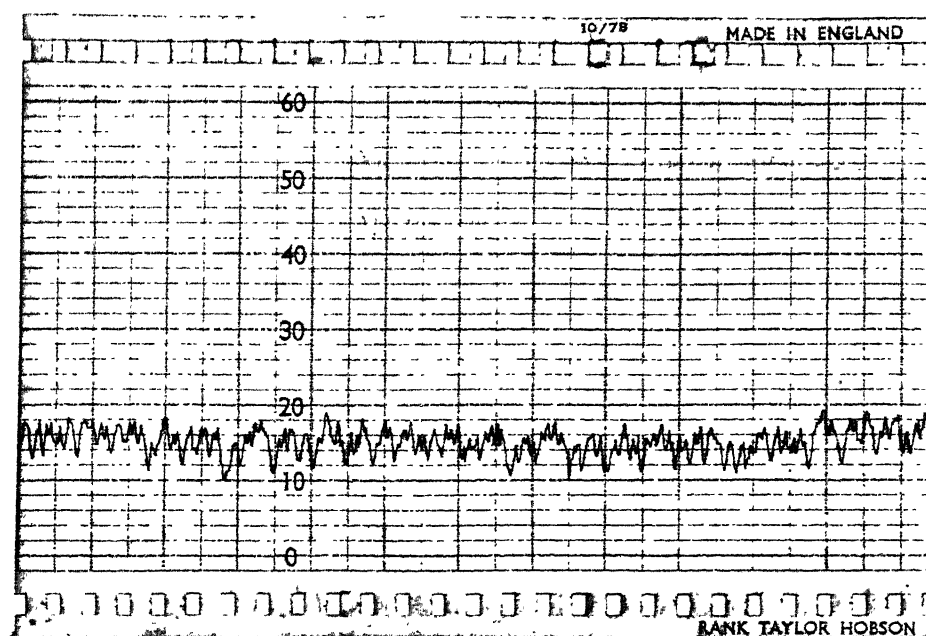
(a) SPECIMEN NO. MA-2
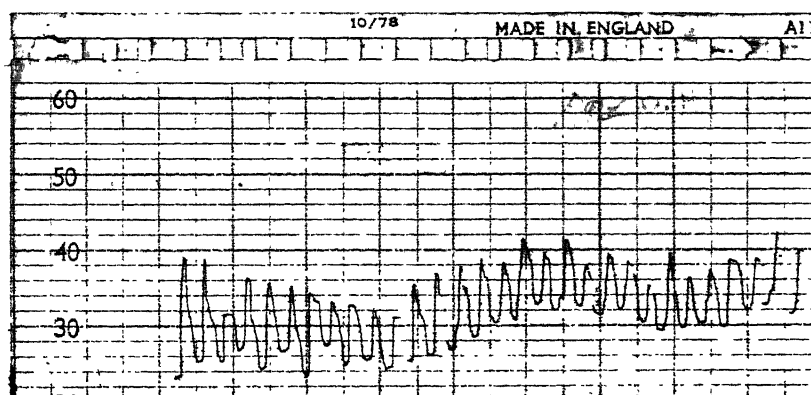
(b) SPECIMEN NO. FA-2

HORIZOTAL MAGNIFICATION=20
VERTICAL MAGNIFICATION=1000

FIG. 4.8   SURFACE   PROFILE BY TALYSURF—10

ROUGNESS MEASURING INSTRUMENT

specularly at near grazing angles of incidence. Small amount of light is reflected in specular direction at less than 80° angle of incidence. Table 4.1 gives the theoretical and approximate experimental angle of incidence (θ_{ir}) for which the specular intensity begins to rise for different value of roughness. The lower-theoretical values of θ_{ir} for specimen no. MA-9 and MA-10, Figure 4.7-e and 4.7-f are probably due to the fact that surfaces are much smoother theoretically, with theoretical R_a = 0.14μ and 0.08μ respectively. Experimental and theoretical I_s variation for specimen MA-5 to MA-8 show a reasonable agreement. Further more for specimen MA-9 and MA-10 the theoretical curves, assuming traingular profile are away from the experimental curves. It is expected that for circular profile the theoretical curve is likely to move towards right due to the fact that the variation of I_s with θ_i follows a Bessel function (Figure 4.10).

The variation of I_s with roughness is shown in Figure 4.11 for θ_i = 85° and θ_i = 87.5^O. It is seen that the specular intensity decreases with roughness in both the cases. The decrease is much steeper for θ_i = 85°, furthermore there is a large scatter of datafor θ_i = 87.5^O. The intensity decreases exponentially for θ_i = 85°. The relation given in figure 4.11 can be used to relate I_s for measuring R_a ranging from 0.3 to 1.0 μm, as the intensity does not vary appreciably beyond 1.0 μm which is the order of wavelength of He-Ne laser.

The ratio R_{15} of intensity in the specular direction I_s to the intensity in the direction 15 degrees off-specular I_{15} is plotted against roughness for various values of $\theta_i (25^O, 50^O, 75^O)$ in figure 4.12. In general, R_{15} show a steep fall upto R_a = 4 μm

R_N = NOSE RADIUS

C_e = EFFECTIVE END
      CUTTING EDGE ANGLE

C_s = EFFECTIVE SIDE-
      CUTTING EDGE ANGLE

R_N = 0.25 mm to 1.25 mm

(a) TOOL GEOMETRY

$$h = \frac{(feed)^2}{8 R_N}$$
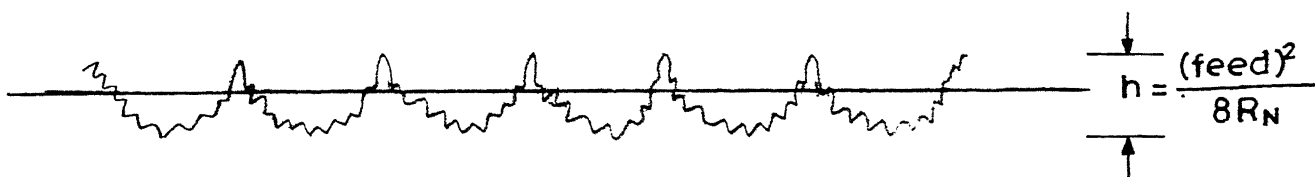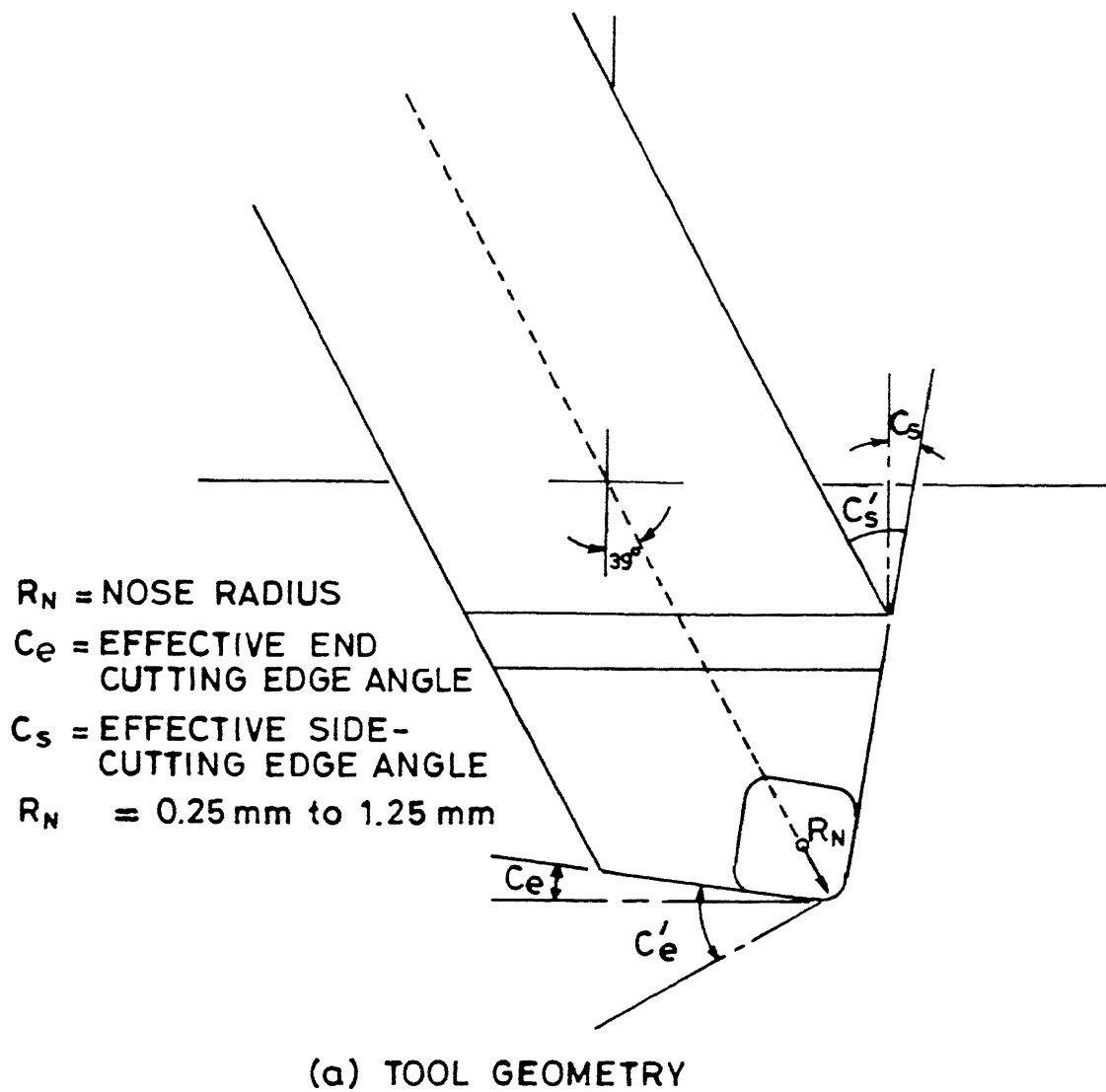
(b) CIRCULAR PROFILE WITH MICRO IRREGULARITIES

FIG. 4.9 PROFILE DUE TO FINITE TOOL RADIUS.

TABLE 4.1

ANGLE OF RISE (θ_{ir})

Specimen No.	Theoretical Roughness $R_a \mu$	Angle of Rise θ_{ir} (Degrees)	
		Theoretical	Experimental
MA-5	3.97	90°	85°
MA-6	1.49	89°	80°
MA-7	0.617	89°	80°
MA-8	0.96	89°	80°
MA-9	0.144	60°	80°
MA-10	0.08	40°	80°

$$J_o^2(X) \ \& \ Sinc^2(X)$$

Dashed = Bessel function $J_o^2(X)$
Solid = $Sinc^2(X)$ = $(Sin(X)/X)**2$

X

FIG. 4.10.   SINC^2(X)   &   J$_o^2$(X)
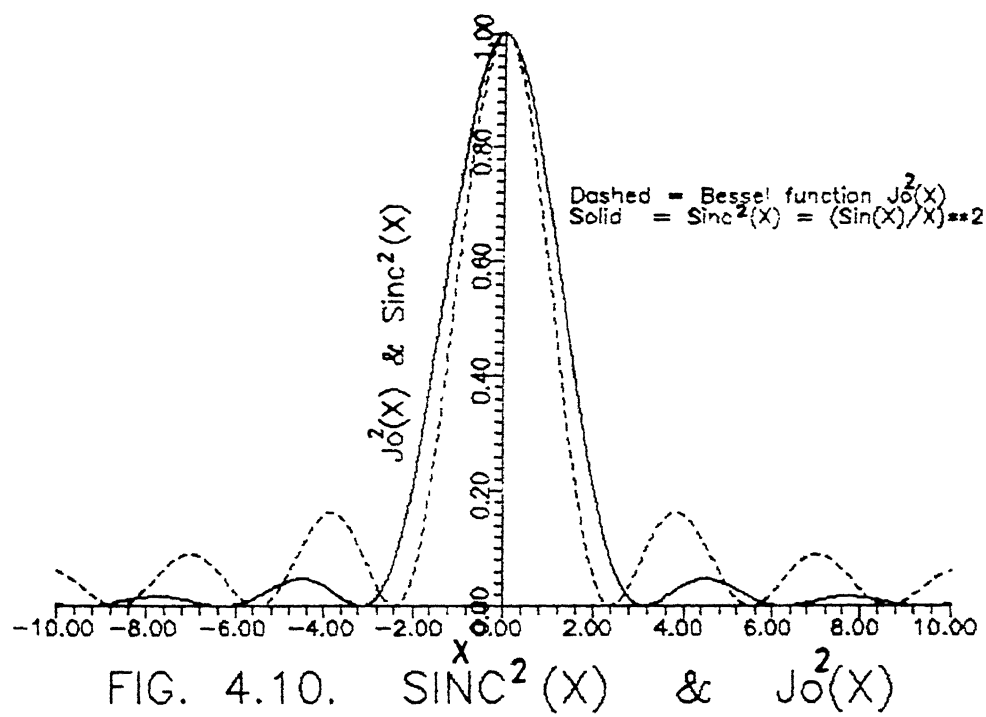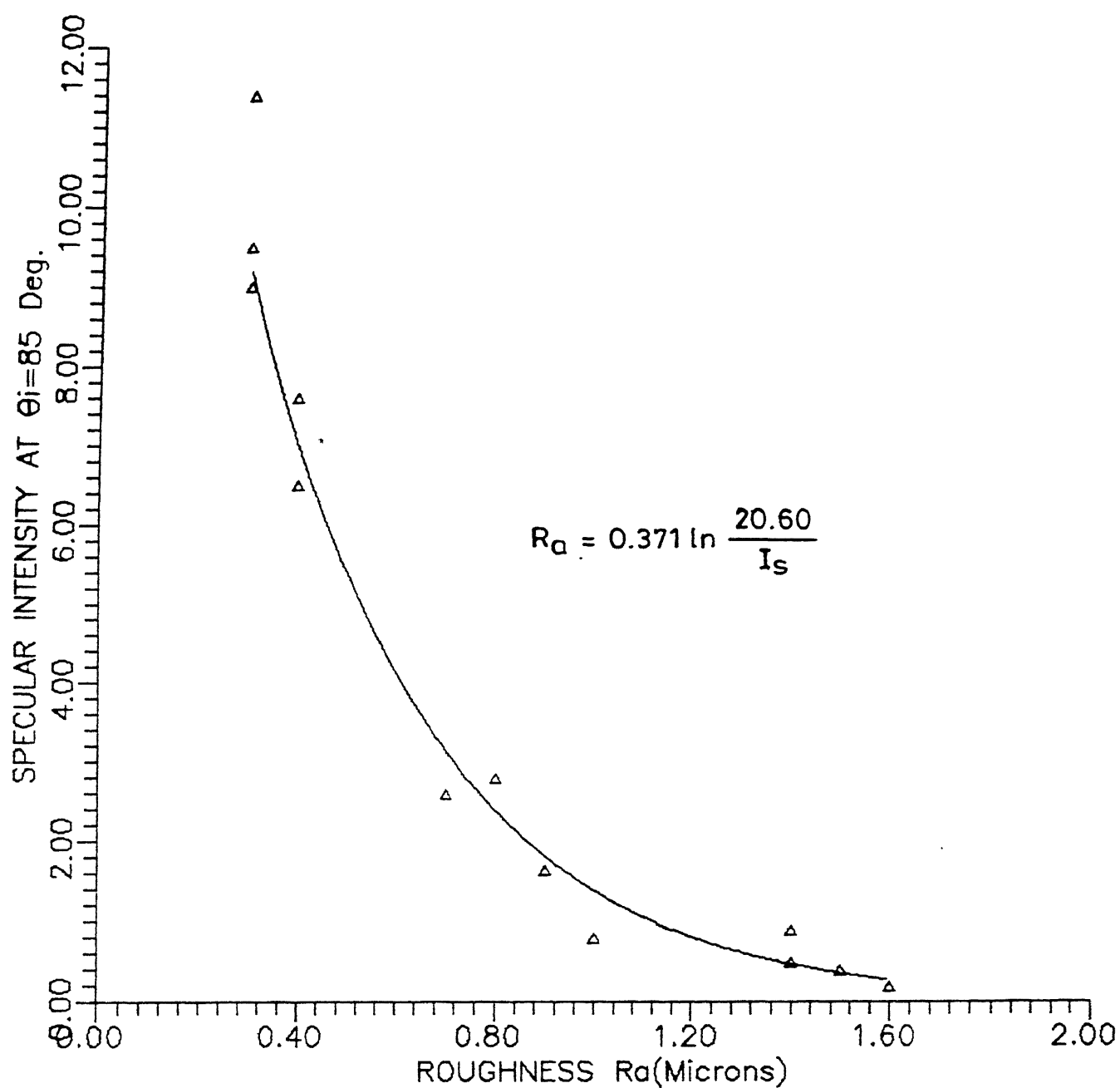
FIG. 4.11-a   VARIATION OF SPECULAR INTENSITY
               WITH ROUGHNESS Ra : $\theta_i = 85°$

$$R_a = 1.732 \ln \frac{24.93}{I_s}$$
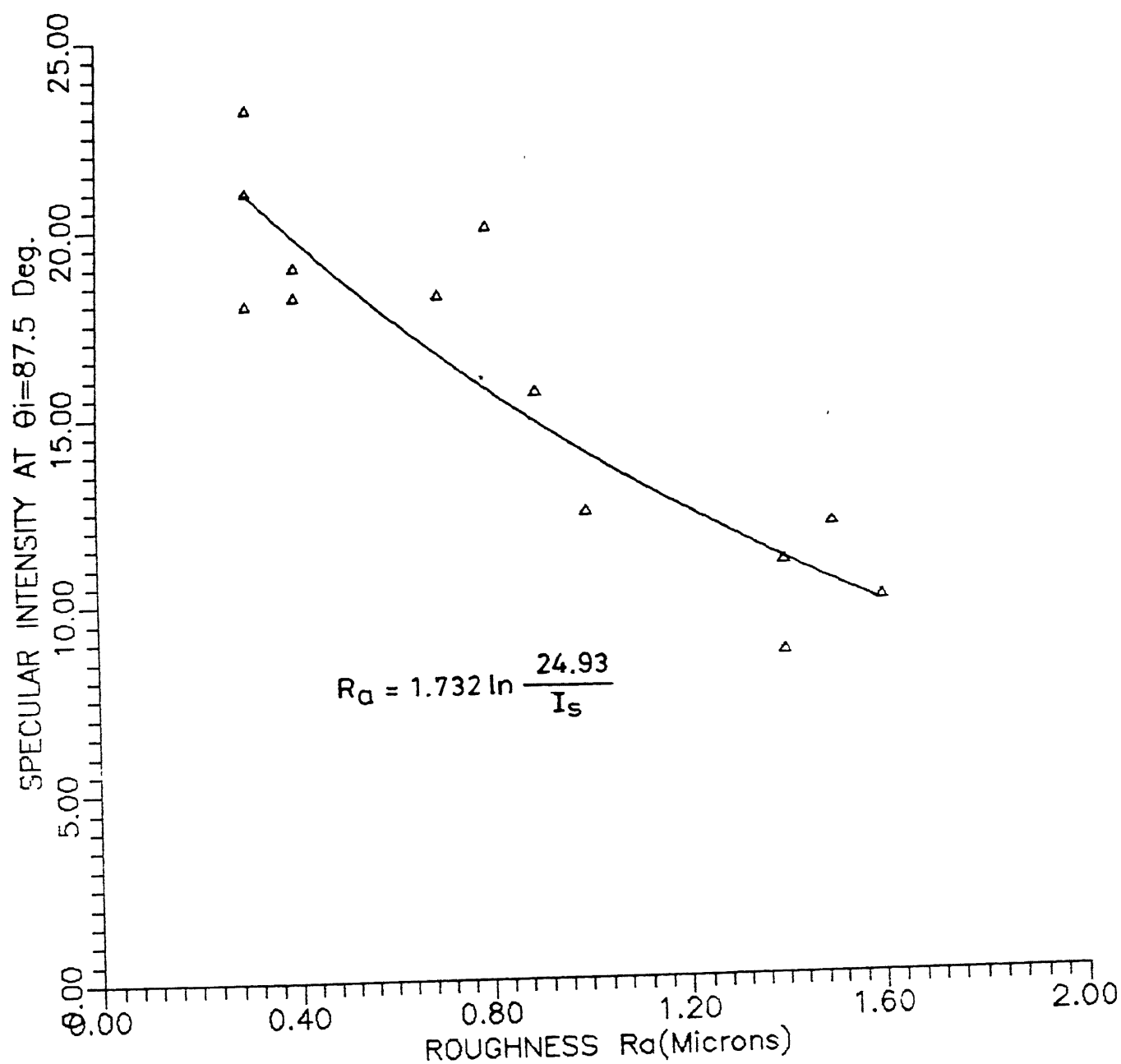
FIG. 4.11-b   VARIATION OF SPECULAR INTENSITY WITH ROUGHNESS R_a : $\theta_i = 87.5°$
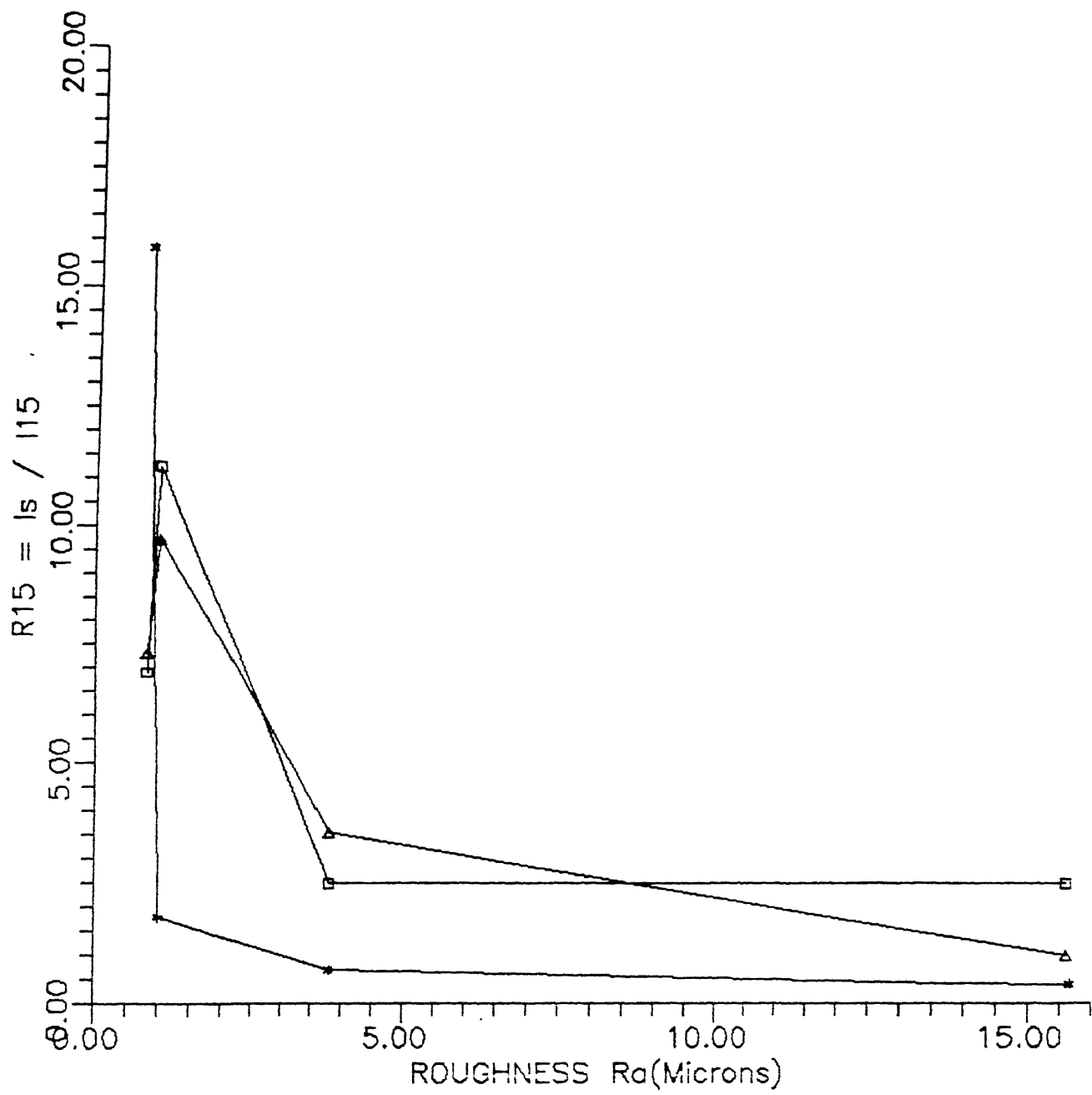
FIG. 4.12.   VARIATION OF INTENSITY RATIO
Is/I15 WITH ROUGHNESS Ra

and there is a little change beyond this value. Certain research workers [9,11] have also the use of R_{30} and R_{40} for measurement of roughness R_a less than λ. However due to limited exprimental results it is not possible to relate R_{15} with roughenss in the present case.

CHAPTER 5

CONCLUSIONS

All the AD plots show a No. of peaks, which are very prominent for higher value of roughness. However, the average experimental spacing are much higher than the theoretical spacing of peaks. Therefore it is not possible to relate the peak spacing from AD plots to the spatial wavelength of surface.

Variation of specular intensity I_s with angle of incidence show that all surfaces tend to reflect most of the incident light specularly at near grazing angles of incidence. Experimental and theoretical I_s variation show a reasonable agreement.

The variation of I_s with roughness show that specular intensity decreases with roughness. The decrease is much steeper for $\theta_1 = 85^\circ$ than for $\theta_1 = 87.5^\circ$. The relation given in figure 4.11 can be used to relate I_s for measuring R_a ranging from 0.3μ to 1.0μ at near grazing angle of incidence of 85°.

The possibility of relationship between R_{15} (ratio of intensity reflected in specular direction to intensity reflected in an 15° off-specular direction) and roughness cannot be found from limited experimental results.

SUGGESTIONS FOR FURTHER WORK

In the present work, experiments are done with aluminium surface with periodic irregularities. This can be extended to other materials also. Another extension of the work can be the study of random rough surfaces using He-Ne laser. Furthermore the

scattered intensity measuring instrument can be mechanised by attaching a stepper motor to it. The detector itself can be mounted on an assembly to enable it to rotate about Y-axis for the study of scattered intensity in three dimensions.

APPENDIX

(A)   BESSEL FUNCTION

$$J_m(x) = \sum_{s=0}^{\infty} \frac{(-1)^s}{s!(m+s)!}(x/2)^{m+2s}$$

Where $(m+s)! = \Gamma(m+s+1) = \int_0^{\infty} e^{-t} t^{m+s} \, dt$

(B)   SINC FUNCTION

$$Sinc(x) = \frac{\sin(x)}{x}$$

(C) PROGRAMME TO CALCULATE $J_0(x)$, sinc(x) and eq. No. (25)

SECTION 2.2.1b

```
c_____
c            This programme is for SPECULAR direction only !
c       Programme wrtn  by Rajnish Kashyap under the supervision of
c   Dr.G.S.Kainth(prof. Mech.) & Dr.K.K.Sharma(Head CELT ) IIT.kanpur
c              . . . . . . . . . . . . . . . .
c              . . . . . . . . . .
c_____
              implicit  double precision (a-h,o-z)
                    open(unit=22,file='bessel')
                    open(unit=23,file='sinc')
                    x=-10.0
                    do 999 kk=0,200
c_____
c              bessel function calculation
c_____
                    rhob=1
                    do 10 i=1,100
                    prod1=1
                    do 20 j=1,i
                    d=float(j)
                    b=(x/2.0)/d
                    prod1=prod1*b
20                  continue
                    prodb=prod1*(-1)**i*prod1
                    rhob=rhob+prodb
10                  continue
                    db=rhob**2
c_____
c              sinc function calculation
c_____
                    prods=(dsin(x))/x
                    dbs=prods**2
                    write(23,11) x,dbs
                    write(22,11) x,db
                    x=x+.1
11                  format(1x,f8.3,4x,f8.5)
999                 continue
                    stop
                    end
```

```
c_____
c       This programme calculates the theoretical intensity distribution
c       due to scattering by a triangular wave.This programme is written
c       by    RAJNISH KASHYAP       8811606 M.Tech.LASER Technology IIT.K
c_____
        implicit double precision (a-h,o-z)
        common t1,rkh,sk,ratio,r11,r12,rl,r21,nen
        dimension t22(10,200),ri(10,200)
        open(unit=21,file='new.out')
        open(unit=22,file='cash.dat1')
c........hene=wavelength of he ne laser.....
c........sk = propagation vector =2pi/lambda......
        r=200.0
c    ...  r=distance  of  detector  from  the  specimen .....
        rewind 22
        a=3.1415925/180.0
        hene=6328.193e-07
        sk=2.0*3.1415925/hene
        do 67 j=1,7
c........2h= height  of  the  triangular  wave ........
        r21=1.8
        read(22,*,end=90)feed,rpm,phi11,phi22,t
        write(21,10)feed,rpm,phi11,phi22,t
        phi1=phi11*a
        phi2=phi22*a
        rl=feed/rpm
        ratio=rl/hene
        h=(rl/2.0)/((1/dtan(phi1))+(1/dtan(phi2)))
        r11=2.0*h/dtan(phi1)
        r12=rl-r11
        rkh=sk*h
        t1=t*a
        nen=r21/(rl*dcos(t1))
        r21=rl*float(nen)
        print*,'No. of Triangles=',nen,'    Base of beam=',r21
c........ ..           1.8 =dia of the  laser  beam...................
c... ........           at  the  base  at the point of incidence .......
c ..  ..                    ...loop .  .   ....   .........................
        t21=t-45.0
        tt=t+45.0
        if(tt.gt.90)then
        mt=((90.0-t)*2.0)+(45.0*2.0)+2.0
        else
        mt=182
        endif
        do 45 m=2,mt
        t22(j,m)=t21
        t2=t22(j,m)*a
        x=rl/2.0
        mu=0
        real=0
        rimag=0
        do 55 n=0,(nen-1)
        t2x=datan(((r21/2.0)-x)/(r*dcos(t2))+dtan(t2))
        call intensity(t2x,mu,x,freal,fimag)
        real=real+freal
        rimag=rimag+fimag
        x=x+rl
        mu=mu+1
55      continue
        ri(j,m)=(real**2+rimag**2)
        t21=t21+0.5
45      continue
c...... subroutine for the calculation of max.Value.................
                                        . . . . . . . . . . . .
```

```fortran
          m=2
          rmax=0
20        if(ri(j,m).gt.rmax)rmax=ri(j,m)
          m=m+1
          if (m.lt.mt)goto 20
          write(21,*)' Rmax.=',rmax
c.... .....           ...... NORMALISING................................
          m=2
          do 65 k=2,mt
          ri(j,m)=ri(j,m)/rmax
          m=m+1
65        continue
c ................ ........................ ..............................
          print*.'rmax=',rmax
          write(21,11)'rl=',rl,'h=',h,'rkh='
     1    ,rkh,'n=',nen
          write(21,13)(t22(j,m),ri(j,m),m=2,mt)
67        continue
          stop
90        endfile 22
10        format(1h /1x,'feed=',f9.4,3x,'rpm=',f8.2,3x, 'phi1 =',
     1    f6.2,3x,'phi2  =',f6.2,3x,'incidence='f7.2)
11        format(2x,5(a4,f10.4,3x))
13        format (1h /,6(2x,f6.1,2x,f10.8))
          end
c...... ... .     Subroutine  for  Intensity .......................
c .   .  .  .    .................   .... ..............................
          subroutine intensity(t2x,mu,x,freal,fimag)
          implicit double precision (a-h,o-z)
          common t1,rkh,sk,ratio,r11,r12,rl,r21,nen
c        .       .      Calculation of factor F..................... ...
c.        F=F2(C1,O2):page 25 eq.45 of the book.. ...................
          t2xx=(t2x/3.1415925)*180.0
          f=((1+dcos(t1+t2x))/((dcos(t1)+dcos(t2x))*dcos(t1)))
c. .      p=p of the book , p no 38 eq.13.........................
          p=ratio*(dsin(t1)-dsin(t2x))
c.       . Vx=vx of the book,p no 48.eq.no. (4)....................
          vx=sk*(dsin(t1)-dsin(t2x))
c... .. ... x1=Vz h of the book,p no.48:eq.no.7....................
          x1=-rkh*(dcos(t1)+dcos(t2x))
          phi=2 0*3 1415925*p*float(mu)
c.. ... phi = express: on p.no. 39,eq.(14)= e(i*2p*Pi*mu)..........
          c1=vx+(2 0*x1/r11)
          c2=vx-(2 0*x1/r12)
          phi1=c1*r11/2.0
          phi2=(2 0*x1*rl/r12)+(c2*r11)+(c2*r12/2.0)
          r1=(2 0/c1)*dsin(c1*r11/2 0)
          r2=(2.0/c2)*dsin(c2*r12/2.0)
          rx=r1*dcos(phi1)+(r2*dcos(phi2))
          ry=(r1*dsin(phi1))+(r2*dsin(phi2))
          rmag=dsqrt(rx**2+ry**2)/rl
          rphase=datan(ry/rx)
          tphase=rphase+phi
c....     fr=intensity product...............................
          fr=rmag*f/float(nen)
          freal=fr*dcos(tphase)
          fimag=fr*dsin(tphase)
          return
          end
```

REFERENCES

[1] Thomas, T.R., *Rough surfaces*, Longman Inc., 1982,New York.

[2] Takeyama, H., Sekiguchi, H., Murata, R., "IN-Process Detection of Surface in Machinery," CIRP Annals, vol.25, 1976, pp. 467-475.

[3] Tanner, L.H. Fahovm, M., "A Study of the Surface Parameters of Ground and Lapped Metal Surfaces, Using Specular and Diffuse Reflection of Laser Light," Wear, vol.36, 1976, pp. 299-316.

[4] Vorburger, T.V., Teague, E.C., "Optical Techniques for On-Line Measurement of Surface Topography", Precision Engineering, vol. , 1981, pp. 61-84.

[5] Peters, J., Vanherck, P., Sastrodinolo, M., "Assessment of Surface Topology Analysis Techniques, " Annals of CIRP, vol.28/2/1979, pp. 539-554.

[6] Beckmann, P., Spizzichino, A., *The Scattering of Electromagnetic Waves from Rough Surfaces*,Pergamon, New York, 1963.

[7] Bennet, H.E., "Specular Reflectance of Aluminized Ground Glass and the Height Distribution of Surface Irregularities," J. Opt. Soc. Am, vol.53, 1963.

[8] Tanner, L.H., "A Comparison of Talysurf 10 and Optical Meausrements of Roughness and Surface Slope," Wear, vol.57, 1979.

[9] Clarke, G.M., Thomas, T.R., "Roughness Measurement with Laser Scanning Analyser," Wear, vol.57, 1979.

[10] Church, E.L., "The Measurement of Surface Texture and Topography by Differential Light Scattering," Wear, vol.57, 1979, pp. 93-105.

[11] Church, E.L., Jenkinson, H.A., Zavada, J.M., "Measurement of the Finish of Diamond-Turned Metal Surfaces by Differential Light Scattering," Optical Engineering, vol.16, No.4, 1977, pp. 360-374.

[12] Elson, J.M., Bennet, J.M., "Relation Between the Angular Dependence of Scattering and Statistical Properties Surfaces," J. Opt. Soc. Am, vol.69, No.1, 1979, pp.31-47.

[13] Church, E.L. Jenkinson, H.A., Zavada, J.M.,

"Relationship Between Surface Scattering and Microtopographic Features," Optical Engineering, vol.18, No.2, 1979, pp. 125-136.

[14]   Roger, G., Manley, K., Cheryl, L., "Characterising Gastrolith Surface Roughness with Light Scattering," Op. Comm., vol.74, No.5, 1990, pp. 279-283.

[15]   Herbert, P., Numan, M., Vagszegi, Z., "Laser Optical Roughness Measurement, IMEKO Symposium on Laser Application in Precision Measurement," Budapest, 1986.

[16]   Whitley, J.L., Kusy, R.P., Mayhow, M.J., Ruckthal, J.E., Surface Roughness of Stainless Steel and Electroformed Nickel Standards Using a He-Ne Laser," Optics and Laser Technology, vol.19, No.4, 1987, pp. 189-196.

[17]   Landing, L., Adin Mann, J., Edwards, R.V., "Analysis of a Surface Scattering Spectrometer," Journal of Opt. Soc. Am., vol.16, No.11, 1989, pp. 1692-1701.

[18]   Shiraishi, M., Sato, S., "Dimensional and Surface Roughness Controls in a Turning Operation," ASME Journal of Engineering for Industry, vol.112, 1990, pp. 79-83.

[19]   Yoo, S.M., Dornfeld, D.A., Lemaster, R.L., "Analysis and Modelling of Laser Measurement System Performance for Wood Surface," ASME Journal of Engineering for Industry, vol.112, 1990, pp. 66-112.

[20]   Young, D., Vorburger, J., Teague, C., "In-Process and On-Line Measurement of Surface Finish", Annals of CIRP, vol.29/1/1980, pp. 435-440.

[21]   Shiraishi, M., "In-Process Measurement of Surface Roughness in Turning by Laser Beams, "ASME Journal of Engineering for Industry, Jan. 1981, pp. 1-7.

[22]   Elson, J.M., Bennet, J.M., "Relation Between the Angular Dependence of Scattering and the Statistical Properties of Optical Surfaces.

[23]   Thwaite, E.G., "Power Spectra of Rough Surfaces obtained by Optical Fourier Transformation.

[24]   Stover, J.C., "Roughness characterization of Smooth Machined Surfaces by Light Scattering," Appl. Opts., vol.14, 1975.

[25]   Whitehouse, D.J., "Comparison Between Stylus and Optical Methods for Measuring Surfaces," Annals of CIRP, vol.37/20/1988, pp. 649-653.

[26] Gaskill, J.D., *Linear Systems and Fourier Transforms, and Optics*, John Wiley & Sons, New York, 1978.

[27] Grewal, B.S., *Higher Engineering Mathematics*, Khanna Publishers, New Delhi, 1987.

[28] Gradshteyn, I.S., Ryzhik, I.M., *Table of Integrals, Series, and Products*, Academic Press, 1980.

[29] Pandey, P.C., Shan, H.S., *Modern Machining Processes*, Tata McGraw-Hill, New Delhi, 1980.

[30] Schaum's outline series on ,*Machine Design*,McGraw-Hill, Singapore,1983.

[31] Broadmann, R., Optische Werke, G., Thurn, G., "An Optical Instrument for Measuring the Surface Roughness in Production Control," Annals of CIRP, vol. 33/1/1984, pp. 403-406.

[32] Koning, J., Schellekens, P.H.J., McKeown, P.A., "Wavelength Stability of He-Ne Lasers Used in Interferometry: Limitations and Tracebility," Annals of CIRP, vol.28/1/1979, pp. 307-310.

[33] Johnston, G., Manley, Kim., Lemanski, L., "Characterizing Gastrolith Surface Roughness with Light Scattering," Optics Communication, vol.74, No.5, 1990, pp. 279-283.